



Angular Momentum Evolution of Young Stars in the nearby Scorpius–Centaurus OB Association

Samuel N. Mellon^{1,2}, Eric E. Mamajek^{1,3}, Thomas E. Oberst², and Mark J. Pecaut⁴

¹ Department of Physics and Astronomy, University of Rochester, Rochester, NY 14627, USA; smellon@ur.rochester.edu

² Department of Physics, Westminster College, New Wilmington, PA 16172, USA

³ Current address: Jet Propulsion Laboratory, California Institute of Technology, M/S 321-100, 4800 Oak Grove Dr., Pasadena, CA 91109, USA

⁴ Department of Physics, Rockhurst University, Kansas City, MO 64110, USA

Received 2017 February 20; revised 2017 June 2; accepted 2017 June 5; published 2017 July 24

Abstract

We report the results of a study of archival SuperWASP light curves for stars in Scorpius–Centaurus (Sco–Cen), the nearest OB association. We use SuperWASP time-series photometry to extract rotation periods for 189 candidate members of the Sco–Cen complex and verify that 162 of those are members of the classic Sco–Cen subgroups of Upper Scorpius (US), Upper Centaurus–Lupus (UCL), and Lower Centaurus–Crux (LCC). This study provides the first measurements of rotation periods explicitly for large samples of pre-main-sequence (pre-MS) stars spanning the UCL and LCC subgroups. Our final sample of 157 well-characterized pre-MS stars spans ages of ~ 10 –20 Myr, spectral types of $\sim F3$ –M0, and masses of $M \simeq 0.3$ –1.5 \mathcal{M}_{\odot}^N . For this sample, we find a distribution of stellar rotation periods with a median of $P_{\text{rot}} \simeq 2.4$ days, an overall range of $0.2 < P_{\text{rot}} < 8$ days, and a fairly well-defined mass-dependent upper envelope of rotation periods. This distribution of periods is consistent with recently developed stellar angular momentum evolution models. These data are significant because they represent an undersampled age range and the number of measurable rotation periods is large compared to recent studies of other regions. We also search for new examples of eclipsing disk or ring systems analogous to 1SWASP J140747.93-394542.6 (J1407), but find none. Our survey yielded five eclipsing binaries, but only one appears to be physically associated with the Sco–Cen complex. V2394 Oph is a heavily reddened ($A_V \simeq 5$ mag) massive contact binary in the LDN 1689 cloud whose *Gaia* astrometry is clearly consistent with kinematic membership with the Ophiuchus star-forming region.

Key words: binaries: eclipsing – open clusters and associations: individual (Sco–Cen) – starspots – stars: pre-main sequence – stars: rotation

Supporting material: machine-readable tables

1. Introduction

The Scorpius–Centaurus OB Association (Sco–Cen) is the nearest OB association to the Sun ($d \simeq 118$ –145 pc; de Zeeuw et al. 1999; Preibisch & Mamajek 2008). It contains the nearest large sample of 10–20 Myr stars, making it valuable for direct imaging of giant exoplanets and studies of disk evolution. The group is composed of three classically defined subgroups: Upper Scorpius (US; median age $\simeq 11$ Myr), Upper Centaurus–Lupus (UCL; median age $\simeq 16$ Myr), and Lower Centaurus–Crux (LCC; median age $\simeq 17$ Myr; Pecaut et al. 2012; Pecaut & Mamajek 2016). This grouping can be problematic, however, because the boundaries of the subgroups are somewhat ill-defined and each group exhibits a significant substructure (Preibisch & Mamajek 2008; Rizzuto et al. 2012; Pecaut & Mamajek 2016). Most stars located in the three subgroups with masses⁵ of $< 2 \mathcal{M}_{\odot}^N$ are pre-main-sequence (pre-MS), and some are still accreting from protoplanetary disks (e.g., Luhman & Mamajek 2012; Pecaut & Mamajek 2016). Throughout this paper, we refer to the collection of the classic subgroups US, UCL, and LCC as the Sco–Cen OB Association. We refer to the ensemble of active and recent star formation in the vicinity of the Sco–Cen association as the Sco–Cen *complex*, including the young associations in the Oph, Lup, CrA, and Cha

molecular clouds, and the smaller peripheral groups of ~ 5 –10 Myr-old stars (ϵ Cha, η Cha, and TW Hya; Preibisch & Mamajek 2008). These regions represent a large-scale star-formation event that has been occurring over the past ~ 20 Myr, forming discrete subgroups of batches of dozens to thousands of stars during that span. The three classic subgroups likely represent ensembles of numerous smaller star-formation events rather than monolithic bursts of star formation (Pecaut & Mamajek 2016).

The distribution of rotation periods for pre-MS stars in Sco–Cen can provide useful constraints on stellar angular momentum evolution models. The angular momentum evolution of young stars is governed by several processes that work to increase or decrease the rotation speed of the star. During the pre-MS portion of a star’s lifetime, the gravitational contraction lowers the star’s moment of inertia, which can increase the angular rotation speed as a consequence of angular momentum conservation; magnetic disk-locking can also work against this contraction (Irwin et al. 2011; Gallet & Bouvier 2013). Beyond the zero-age main sequence (ZAMS), the moment of inertia changes very slowly and the star’s angular momentum evolution is dominated by braking via magnetized stellar winds and the transfer of angular momentum between the interior and exterior layers of the star causing a steady spin-down for the remainder of the star’s life (Gallet & Bouvier 2015).

In recent years, rotation periods have been measured for hundreds of stars over a wide range of masses (e.g., Hartman

⁵ \mathcal{M}_{\odot}^N is the symbol for the nominal solar mass as defined by IAU Resolution 2015 B3 (Prša et al. 2016; see https://www.iau.org/static/resolutions/IAU2015_English.pdf).

et al. 2008, 2010; Messina et al. 2010; Irwin et al. 2011; Meibom et al. 2011a, 2011b; Gallet & Bouvier 2013, 2015; Moraux et al. 2013; Cargile et al. 2014; Meibom et al. 2015; Douglas et al. 2016). These distributions of rotation periods as a function of stellar age have enabled the development of angular momentum evolution models. These models, which are used to estimate the ages of stars from the earliest pre-MS through the end of the MS, take into account disk-locking, gravitational contraction, stellar winds, and many other factors (e.g., Meibom et al. 2011a; Barnes 2010; Reiners & Mohanty 2012; Bouvier et al. 2014; Cargile et al. 2014; Gallet & Bouvier 2015). Additional large surveys of rotation periods during the post-accretion pre-MS phase can help constrain these angular momentum evolution models because this age range is undersampled (e.g., Gallet & Bouvier 2015).

The work presented in this paper found rotation periods for 189 young stars, 96 of which are newly measured periods (including an outlying K-giant star with a newly measured short activity period). 162 of these stars belong to the three classic subgroups (US, UCL, LCC). 157 of the Sco–Cen members had retrievable spectral types, which were used to estimate the masses of each star. The stars with spectral types were then plotted against current theoretical angular momentum evolution models from Gallet & Bouvier (2015). This study finds that these data are consistent with what these models predict.

This study was also designed to discover and characterize new circumsecondary eclipsing disk/ring systems like the one found around J1407 (Mamajek et al. 2012; Scott et al. 2014; Kenworthy & Mamajek 2015) and new examples of rare pre-MS eclipsing binary stars (e.g., Morales-Calderón et al. 2012; Kraus et al. 2015). No new eclipsing disk systems were discovered. Five candidate eclipsing binary systems were identified. However, upon further scrutiny, only one appears to be associated with Sco–Cen.

This paper is organized as follows. Section 2 discusses the construction of our initial sample of Sco–Cen candidates and details the data used in the survey; Section 3 details the use of periodograms and the generation of phase-folded light curves; Section 4 provides a summary of the study’s results, discusses the rotational periods of the Sco–Cen members, and how these rotational periods help to understand the evolution of low-mass stars.

2. Data

2.1. Sco–Cen Sample and Membership

In the course of previous work on the membership and star-formation history of the Sco–Cen complex (including both the OB subgroups and related young stellar object populations in the associated molecular clouds; see, e.g., Preibisch & Mamajek 2008; Pecaut et al. 2012; Pecaut & Mamajek 2016), an internal database was constructed of 5551 candidate stellar members. For the classic subgroups, candidate members were drawn from the following studies: Ardila et al. (2000), Blaauw (1946), Dawson et al. (2011), de Geus et al. (1989), Hoogerwerf et al. (2000), Lodieu et al. (2006, 2007, 2013), Luhman & Mamajek (2012), Mamajek et al. (2002), Martin et al. (2004), Pecaut et al. (2012), Pecaut & Mamajek (2016), Preibisch & Mamajek (2008), Rizzuto et al. (2012), Sartori et al. (2003), Slesnick et al. (2006), Song et al. (2012), Wichmann et al. (1997), and de Zeeuw et al. (1999). The

quality of membership assignments in these studies is quite heterogeneous. Some were selected only by virtue of photometry, proper motions, and/or X-ray emission. Many were also vetted using parallaxes and proper motions from the first *Gaia* data release (Gaia Collaboration et al. 2016). Given the large number of candidate members, memberships were only reassessed if a star passed several criteria summarized in Section 3.1.2.

2.2. Photometry

2.2.1. SuperWASP Photometry

In order to estimate both long-term median magnitudes and rotational periods (i.e., periodic variations in magnitudes due to starspot rotation) for Sco–Cen stars, these 5551 candidate members were cross-referenced with the archival single-band time-series photometric data catalog from the Super Wide Angle Search for Planets (SuperWASP). SuperWASP consists of two robotic observatories in La Palma, Spain, and Sutherland, South Africa. Each observatory has a bank of eight wide-angle cameras that collectively provide a 490 deg² field of view (FOV) per pointing at 13'' pix⁻¹ scale within a magnitude range of 8 < V < 13. The observatories have been operating simultaneously and year-round since 2004 to collect V-band photometry over most of the sky with a single-position cadence of approximately 10 minutes (Pollacco 2006; Butters et al. 2010; Smith & WASP Consortium 2014).

The first and only SuperWASP public data release includes data collected between 2004 and 2008. It is available for download via the NASA Exoplanet Archive operated at the NASA Exoplanet Science Institute.⁶ The data were processed via the SuperWASP pipeline and post-pipeline analysis including astrometric calibration, aperture photometry, and photometric calibration. The data are provided in *.FITS and *.tbl formats, the latter containing observation timestamps (HJD), magnitudes calibrated to the Tycho-2 V_T system, and their uncertainties (Pollacco 2006; Butters et al. 2010). SuperWASP fields in the Sco–Cen region were covered over three ~100 day seasons between 2006 and 2008. Of the 5551 candidate Sco–Cen members, 1689 of them were found to have SuperWASP counterparts.

A data reduction and periodogram analysis pipeline was used to process SuperWASP time-series photometry (described in Section 3.1) for each of the 1689 candidate stars. Table 1 contains the raw results from 1689 light curves, which includes the strongest periods (excluding obvious aliases) and fitted amplitudes for these periods from each season.

Only 189 of them were found to have rotation periods that were consistent throughout at least two of the 2006–2008 seasons. Of those 189 stars, 162 of them were confirmed as members of classic subgroups (plotted in Figure 1, see Section 2.2.2). Table 2 contains the reduced period and stellar information for these 162 stars. This sample is further trimmed to 157 stars for aspects of the analysis requiring spectral types since seven of the stars do not have a measured spectral type.

The remaining 27 stars belong to associated younger star-forming regions in the Sco–Cen complex, namely the Lup, Oph, and CrA regions (and two foreground members of the TW Hya association and a background Li-rich K giant). These 27 stars were not used in the subsequent analysis because their

⁶ <http://exoplanetarchive.ipac.caltech.edu/>

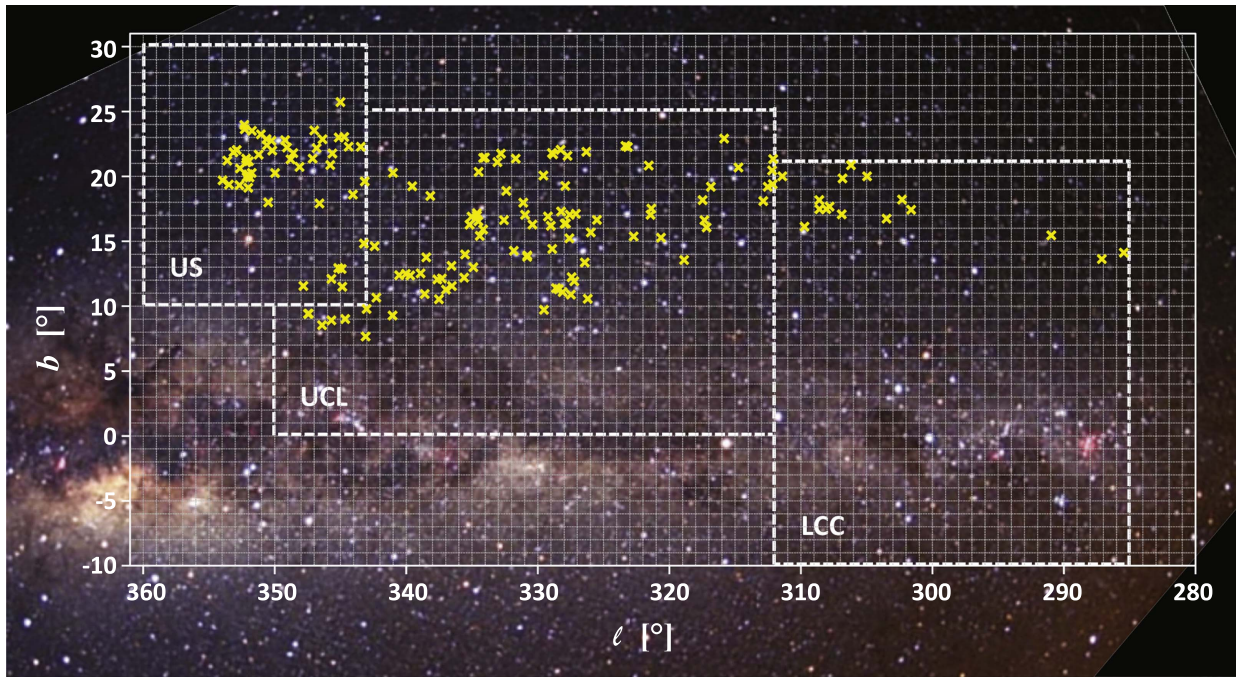


Figure 1. The distribution of Sco-Cen members with rotation periods plotted in Galactic Coordinates (yellow crosses). The background is a wide field optical image of the Sco-Cen region taken by Fred Espenak (NASA GSFC; <http://www.mreclipse.com>). The classic Sco-Cen subgroup boundaries defined by de Zeeuw et al. (1999) are plotted as dashed white lines.

Table 1
Periodogram Analysis Results

ISWASP (J)	Season Start (HJD)	Season End (HJD)	Period (Days)	Amplitude (Mag)
111327.46-452332.7	2453860.2218	2453924.2104	0.628	0.038
111327.46-452332.7	2454105.5074	2454307.2128	0.628	0.035
111327.46-452332.7	2454467.4436	2454614.2497	0.628	0.039
111434.43-441824.1	2453860.2219	2453924.2103	0.974	0.067

Note. This table contains all of the rotation period information extracted from the complete 1689 star sample. The remainder of the table is available electronically. Each entry is for one SWASP object for a single season between the reported HJD dates. For each season, we report the identifiers, season HJDs, strongest period(s) in that season, and the amplitude of the phase-folded light curve.

(This table is available in its entirety in machine-readable form.)

numbers are small (the effects of extinction are likely greatly reducing the coverage of members of these star-forming regions in SuperWASP catalog). These stars are compiled in Table 3, including their statistically significant periods.

2.2.2. Multi-band Photometry

Due to the large pixel size of the SuperWASP survey ($13''.7 \text{ pixel}^{-1}$), the median V_T magnitude may represent the unresolved light from multiple stars, which can result in spurious estimates of colors, reddening, and extinction (see Section 3.2). Thus, in addition to SuperWASP single-band time-series photometry, multi-band single instance (non-time-series) photometry from the archival databases of the Two Micron All-Sky Survey (2MASS; Cutri et al. 2003b; Skrutskie et al. 2006), the fourth United States Naval Observatory CCD Astrograph Catalog, (APASS; Henden et al. 2012), and the Yale/San Juan Southern Proper Motion Catalog 4 (SPM4; Girard et al. 2011) were used. These data were employed for three purposes: (1) to convert SuperWASP’s Tycho-2 V_T magnitudes to Johnson V_J magnitudes; (2) to help verify

the membership of our Sco-Cen candidates; and (3) to obtain accurate V -band magnitudes for estimates of observed colors, estimated reddenings, and HR diagram placement for the target stars.

To convert SuperWASP’s Tycho-2 V_T magnitudes to the Johnson V_J system, two linear trends were fit to the Tycho-2 (Høg et al. 2000) and 2MASS (Skrutskie et al. 2006) photometry for nearby ($d < 75 \text{ pc}$) *Hipparcos* stars, whose absolute magnitudes were within 1 mag of the main sequence and whose photometric errors were $< 0.03 \text{ mag}$ in the relevant bands:

$$V_J - V_T = -0.095 - 0.062(V_T - J - 1.631) \quad (1)$$

$$V_J - V_T = -0.083 - 0.049(V_T - H - 1.791). \quad (2)$$

The uncertainties in the zero-points are 0.001 mag, and uncertainties in the slopes are 0.002, while the rms dispersions in the fits are 0.01 mag. The fits are well-constrained over the color ranges $0 < (V_T - J) < 3.6$ and $0 < (V_T - H) < 4.2$.

While cross-referencing the SuperWASP and 2MASS data, we found that, for approximately one-third of the stars in our

Table 2
Data for Sco-Cen Members

1SWASP (J)	2MASS (J)	Subgroup	Period (days)	SpT	References	V (mag)	K_S (mag)	A_V (mag)	$(V - K_S)_0$ (mag)	T_{eff} (K)	M/M_{\odot}
111327.46-452332.7	11132622-4523427	LCC	0.628 ± 0.002 ^a	M0.5	1	12.83	8.50	0.278	4.090	3700	0.56
112102.95-462630.9	11210295-4626308	LCC	3.798 ± 0.844 ^a	11.09	8.96	0.194 ^c	1.935
114445.40-455106.2	11444540-4551062	LCC	2.166 ± 0.016	9.94	8.57	0.194 ^c	1.174
124419.32-452523.3	12441932-4525235	LCC	3.122 ± 0.044	F9V	3	9.60	8.00	0.279	1.350	6090	1.35
124807.78-443916.7	12480778-4439167	LCC	1.048 ± 0.005 ^a	G7V	4	9.98	7.51	0.576	1.950	5290	1.20
125431.43-460736.4	12543141-4607361	LCC	1.047 ± 0.006 ^a	G0	6	9.88	7.91	0.666	1.370	6050	1.34
130154.38- 424942.0	13015435-4249422	LCC	2.612 ± 0.016	K3IV	2	11.89	9.10	0.045	2.795	4550	1.019
130750.08-415433.1	13075009-4154331	LCC	0.837 ± 0.004	F5.5V	3	9.68	8.25	0.261	1.200	6335	1.39
131129.06-425241.7	13112902-4252418	LCC	6.133 ± 0.186 ^a	M0Ve	2	13.60	9.24	0.393	4.353	3770	0.611
131307.12-453743.6	13130714-4537438	LCC	5.666 ± 0.166	K5Ve	6	11.61	8.33	0.000	3.281	4140	0.85
131746.91-445653.1	13174687-4456534	LCC	0.409 ± 0.001	K5IVe	2	12.08	8.83	0.000	3.243	4140	0.85
131913.71-450632.7	13191370-4506326	LCC	3.088 ± 0.045	K5IVe	2	11.92	9.07	0.000	2.844	4140	0.85
132137.28-442151.3	13213722-4421518	LCC	1.124 ± 0.005 ^a	M0.5	1	12.91	8.85	0.000	4.067	3700	0.56
132204.46-450323.1	13220446-4503231	LCC	1.299 ± 0.008	G0V	4	10.06	8.54	0.162	1.370	6050	1.34
132917.63-461422.8	13291766-4614230	LCC	3.675 ± 0.065	K5IVe	2	12.17	9.23	0.000	2.939	4140	0.849
133431.89-420930.7	13343188-4209305	LCC	0.502 ± 0.001 ^b	K2IVe	6	10.38	8.09	0.000	2.285	4760	1.081
133640.98-404336.3	13364090-4043359	UCL	1.916 ± 0.016	K6IVe	2	12.55	9.06	0.000	3.488	4020	0.78
133757.29-413441.9	13375730-4134419	UCL	4.796 ± 0.112 ^a	K1IV	4	10.09	7.88	0.000	2.208	4920	1.12
133849.37-423723.3	13384937-4237234	UCL	8.572 ± 0.280	K3.5IV	2	11.45	8.89	0.000	2.556	4440	0.982
134055.89-424450.2	13405585-4244505	UCL	1.995 ± 0.023	K8IVe	2	12.32	9.12	0.000	3.198	3940	0.729
134355.67-434540.3	13435567-4345403	UCL	1.887 ± 0.017 ^a	F8IV	3	9.64	7.70	0.674	1.340	6100	1.35
135006.28-405008.8	13500627-4050090	UCL	1.416 ± 0.012 ^b	G0V	4	10.09	8.16	0.620	1.370	6050	1.34
135220.48-382534.4	13522045-3825345	UCL	1.748 ± 0.014	M1.5	1	13.20	8.92	0.000	4.286	3560	0.45
140220.72-414450.8	14022072-4144509	UCL	3.349 ± 0.048 ^a	G9IV	4	10.62	8.40	0.137	2.100	5120	1.16
140701.16-423300.6	14070116-4233007	UCL	1.704 ± 0.013 ^a	G3V	3	10.06	8.58	0.000	1.479	5740	1.29
140856.07-440348.0	14085608-4403488	UCL	0.784 ± 0.026	K3IVe	2	11.47	8.52	0.193	2.943	4550	1.019
140903.57- 443844.3	14090357-4438442	UCL	1.242 ± 0.006	F8V	4	9.46	7.88	0.268	1.340	6100	1.35
142130.55-384525.4	14213051-3845252	UCL	4.326 ± 0.289	K6IVe	2	12.12	8.87	0.000	3.250	4020	0.780
142243.62-462805.2	14224364-4628054	UCL	0.953 ± 0.005 ^a	K2.5IV(e)	2	11.56	9.10	0.000	2.466	4655	1.05
142544.46-365246.2	14254446-3652461	UCL	0.425 ± 0.001	F9.5V	7	9.67	8.06	0.289	1.350	6095	1.35
142621.35-364405.8	14262134-3644057	UCL	2.155 ± 0.021	K0IV	2	10.56	8.51	0.000	2.048	5030	1.14
142702.67-415351.0	14270268-4153511	UCL	2.322 ± 0.192	F9V	3	9.71	8.09	0.308	1.350	6090	1.35
142809.30-441417.4	14280929-4414175	UCL	5.299 ± 0.227 ^a	G5V	4	9.92	7.79	0.396	1.770	5500	1.24
142819.37-421934.0	14281937-4219341	UCL	0.956 ± 0.004	G2V	4	10.31	8.39	0.479	1.490	5870	1.31
143808.68-432200.3	14380862-4322008	UCL	5.909 ± 0.232	K7IVe	2	12.72	8.89	0.240	3.620	3970	0.75
143945.49-360044.3	14394548-3600443	UCL	2.407 ± 0.028	10.87	8.35	0.194 ^c	2.341
144619.03-354146.5	14461903-3541464	UCL	0.183 ± 0.001 ^b	F6V	7	9.72	8.30	0.200	1.250	6250	1.38
144723.44-350313.4	14472343-3503134	UCL	3.66 ± 0.056	K3	8	11.55	8.93	0.000	2.616	4550	1.02
144813.20-410258.9	14481320-4102590	UCL	2.622 ± 0.028 ^a	K2	8	11.14	8.62	0.031	2.490	4760	1.08
145025.81-350648.6	14502581-3506486	UCL	1.660 ± 0.014 ^a	K1IV	4	10.59	8.11	0.183	2.320	4920	1.12
145035.11-345905.2	14503508-3459056	UCL	3.208 ± 0.044 ^a	K4	8	11.99	8.88	0.055	3.060	4330	0.94
145226.27-374008.0	14522619-3740088	UCL	3.762 ± 0.060	K3	8	12.04	9.23	0.073	2.750	4550	1.02
145241.97-414155.1	14524198-4141552	UCL	0.792 ± 0.003 ^b	K3IV	4	11.17	8.29	0.150	2.750	4550	1.02
145411.20-395523.4	14541121-3955233	UCL	3.361 ± 0.044	K2	8	11.65	9.00	0.181	2.490	4760	1.08
145625.72-394616.5	14562573-3946170	UCL	6.886 ± 0.373	M2	8	14.29	10.04	0.000	4.251	3490	0.39
145719.62-361227.4	14571962-3612274	UCL	2.372 ± 0.026 ^b	G3V	4	10.28	8.28	0.468	1.580	5740	1.29
145837.56-391502.6	14583744-3915033	UCL	3.236 ± 0.117 ^a	M0IVe	2	13.01	8.65	0.400	4.360	3770	0.611

Table 2
(Continued)

1SWASP (J)	2MASS (J)	Subgroup	Period (days)	SpT	References	V (mag)	K_S (mag)	A_V (mag)	$(V - K_S)_0$ (mag)	T_{eff} (K)	M/M_{\odot}
145922.76-401312.0	14592275-4013120	UCL	1.612 ± 0.022 ^b	G8(IV)	3	10.04	7.96	0.309	2.020	5210	1.18
145952.44-401159.5	14595244-4011594	UCL	1.164 ± 0.005 ^b	F8V	7	10.00	8.40	0.284	1.340	6100	1.35
150051.88-433121.0	15005189-4331212	UCL	3.641 ± 0.095 ^a	K1IV	4	11.20	8.73	0.159	2.320	4920	1.12
150111.55-412040.5	15011155-4120406	UCL	0.906 ± 0.004 ^a	G0V	4	10.30	8.32	0.684	1.370	6050	1.34
150226.03-340513.0	15022600-3405131	UCL	2.790 ± 0.033	K4	8	12.21	9.28	0.000	2.928	4330	0.94
150353.23-390625.2	15035213-3906283	UCL	4.354 ± 0.280 ^b	K6Ve	2	11.81	8.56	0.000	3.254	4020	0.780
150448.91-394923.6	15044891-3949235	UCL	2.371 ± 0.045 ^b	F8	8	9.76	8.16	0.291	1.340	6100	1.35
150544.24-331250.7	15054424-3312508	UCL	2.742 ± 0.104	K4IVe	2	12.24	9.23	0.252	3.002	4330	0.938
150737.74-460315.5	15073774-4603156	UCL	2.442 ± 0.043	K2	9	11.51	9.10	0.000	2.412	4760	1.08
150825.00-333755.4	15082502-3337554	UCL	6.570 ± 0.200	K7/M0	8	12.71	9.17	0.000	3.546	3910	0.71
150837.74-442316.9	15083773-4423170	UCL	0.311 ± 0.001 ^a	G6IV(e)	2	10.61	8.81	0.000	1.805	5390	1.22
150838.50-440052.1	15083849-4400519	UCL	1.011 ± 0.004	G0V	4	10.50	8.45	0.771	1.370	6050	1.34
150853.74-371546.4	15085379-3715467	UCL	2.615 ± 0.028	K5	9	11.99	9.00	0.000	2.990	4140	0.85
150911.67-412427.6	15091168-4124275	UCL	4.382 ± 0.068	10.44	9.01	0.194 ^c	1.246
151029.53-390256.6	15102954-3902566	UCL	2.824 ± 0.032	K3IV(e)	2	11.64	9.27	0.000	2.366	4550	1.02
151049.46-380748.3	15104947-3807483	UCL	0.464 ± 0.004	A9/F0IV/V	7	9.74	8.30	0.859	0.680	7360	1.45
151104.53-325130.5	15110450-3251304	UCL	3.485 ± 0.051 ^a	K6	8	11.79	8.67	0.000	3.119	4020	0.78
151136.98-355041.5	15113696-3550417	UCL	4.485 ± 0.084	K5	8	12.43	9.33	0.000	3.100	4140	0.85
151139.69-324855.8	15113968-3248560	UCL	3.914 ± 0.068	M1.5	8	13.78	9.38	0.050	4.360	3560	0.45
151250.18-450804.5	15125018-4508044	UCL	2.501 ± 0.027 ^a	G2V	4	10.46	8.71	0.291	1.490	5870	1.31
151509.35-443836.0	15150933-4438362	UCL	6.004 ± 0.157	M0	9	13.71	9.86	0.000	3.848	3770	0.61
151545.36-333159.7	15154537-3331597	UCL	2.275 ± 0.023 ^a	K0e	6	10.70	8.38	0.144	2.190	5030	1.14
151552.73-441817.4	15155274-4418173	UCL	2.403 ± 0.025 ^b	K1	8	12.49	9.45	0.801	2.320	4920	1.12
151636.70-440720.4	15163663-4407204	UCL	0.406 ± 0.001	K2	9	11.97	9.19	0.324	2.490	4760	1.08
151826.90-373802.1	15182692-3738021	UCL	3.121 ± 0.040 ^a	G8IV	4	10.83	8.51	0.338	2.020	5210	1.18
151852.83-405052.6	15185282-4050528	UCL	0.379 ± 0.001	G8	9	10.93	8.55	0.405	2.020	5210	1.18
151915.98-405607.7	15191600-4056075	UCL	2.839 ± 0.032 ^a	K0e	6	11.46	8.83	0.488	2.190	5030	1.14
152211.69-395949.9	15221162-3959509	UCL	0.632 ± 0.002 ^a	K3	9	12.05	9.10	0.228	2.750	4550	1.02
152503.58-360445.4	15250358-3604455	UCL	2.226 ± 0.109 ^a	K1IV(e)	6	10.74	8.32	0.112	2.320	4920	1.12
152533.18-361346.6	15253316-3613467	UCL	0.892 ± 0.021 ^b	K2	9	11.68	8.84	0.389	2.490	4760	1.08
152559.64-450115.8	15255964-4501157	UCL	2.537 ± 0.023 ^a	K0IV	4	10.86	8.90	0.000	1.959	5030	1.14
152625.80-363857.3	15262579-3638576	UCL	0.879 ± 0.006	M2.5	9	13.58	8.96	0.000	4.622	3425	0.34
152652.63-372205.6	15265257-3722062	UCL	6.457 ± 0.257 ^a	M0.5	9	12.96	9.14	0.000	3.817	3700	0.56
152722.97-360409.8	15272286-3604087	UCL	2.013 ± 0.658	K7-M0	9	12.12	8.44	0.000	3.682	3910	0.71
152918.96-373719.9	15291901-3737205	UCL	1.313 ± 0.008 ^a	M3	9	13.66	9.01	0.000	4.645	3360	0.29
152947.26-362837.3	15294727-3628374	UCL	2.705 ± 0.033 ^a	K2IVe	6	11.88	8.97	0.465	2.490	4760	1.08
153423.18-330008.9	15342313-3300087	UCL	5.404 ± 0.149 ^a	K7-M0	9	12.71	9.13	0.000	3.584	3910	0.71
153702.13-313639.7	15370214-3136398	UCL	2.369 ± 0.037 ^a	G5V	4	10.01	7.74	0.558	1.770	5500	1.24
153802.67-380722.8	15380264-3807230	UCL	5.717 ± 1.731 ^a	K5	9	12.32	9.38	0.000	2.941	4140	0.85
153838.26-391655.4	15383827-3916553	UCL	6.296 ± 0.175	K4	9	11.61	8.85	0.000	2.752	4330	0.94
153901.86-295631.3	15390187-2956307	UCL	2.457 ± 0.025	K4	10	13.10	9.52	0.587	3.060	4330	0.94
154357.26-392856.9	15435726-3928568	UCL	2.146 ± 0.026	F8V	7	8.85	7.36	0.165	1.340	6100	1.35
154447.12-381140.6	15444712-3811406	UCL	3.165 ± 0.043	K6Ve	6	11.81	8.51	0.000	3.302	4020	0.78
154944.97-392509.1	15494499-3925089	UCL	1.560 ± 0.015 ^{b d}	K1IV(e)	6	10.59	8.14	0.143	2.320	4920	1.12
154959.21-362957.3	15495920-3629574	UCL	5.404 ± 0.122	K2	9	11.54	8.88	0.181	2.490	4760	1.08
155046.65-382926.8	15504672-3829267	UCL	1.931 ± 0.022	K7	9	13.19	8.90	0.754	3.620	3970	0.75
155219.53-381931.0	15521952-3819313	UCL	2.847 ± 0.206	K7	9	13.03	9.53	0.000	3.505	3970	0.75

Table 2
(Continued)

1SWASP (J)	2MASS (J)	Subgroup	Period (days)	SpT	References	V (mag)	K_S (mag)	A_V (mag)	$(V - K_S)_0$ (mag)	T_{eff} (K)	M/M_{\odot}
155225.88-392051.2	15522589-3920512	UCL	2.114 ± 0.027	K4IVe	2	12.29	9.30	0.000	2.991	4330	0.94
155533.82-370940.4	15553378-3709411	UCL	2.278 ± 0.026	K6	9	12.28	9.17	0.000	3.119	4020	0.78
155659.05-393343.0	15565905-3933430	UCL	2.656 ± 0.048^a	G7IV	4	10.59	8.69	0.000	1.896	5290	1.20
155859.88-364619.8	15585980-3646206	UCL	1.378 ± 0.041	M1.5	9	13.52	9.28	0.000	4.239	3560	0.45
155942.18-383349.9	15594217-3833497	UCL	2.862 ± 0.035	F5.5V	7	9.44	8.09	0.174	1.200	6335	1.39
155949.50-362827.9	15594951-3628279	UCL	2.809 ± 0.037	K3	6	11.13	8.03	0.388	2.750	4550	1.02
160108.96-332014.2	16010896-3320141	UCL	4.448 ± 0.104^a	G5IV	4	10.98	8.53	0.760	1.770	5500	1.2
160159.19-361256.0	16015918-3612555	UCL	1.344 ± 0.008^a	K3	9	11.89	8.85	0.325	2.750	4550	1.02
161358.01-361813.4	16135801-3618133	UCL	2.167 ± 0.020^a	G8V	4	11.07	8.85	0.223	2.020	5210	1.18
161426.40-380759.1	16142637-3807597	UCL	4.740 ± 0.094^a	K7	9	12.57	9.12	0.000	3.445	3970	0.75
161934.43-362411.1	16193446-3624111	UCL	1.653 ± 0.011	G0V	6	9.39	7.80	0.248	1.370	6050	1.34
162730.54-374921.5	16273054-3749215	UCL	2.385 ± 0.025^b	K1.5IV	4	11.01	8.65	0.000	2.362	4840	1.10
162752.33-354700.3	16275233-3547003	UCL	1.272 ± 0.006^a	G6IV	6	9.44	7.62	0.000	1.812	5390	1.22
163142.03-350517.2	16314204-3505171	UCL	2.714 ± 0.042^a	K0V	6	10.67	8.67	0.000	2.000	5030	1.14
163520.57-344853.6	16352051-3448538	UCL	4.361 ± 0.080	10.94	7.84	0.194 ^c	2.914
163522.43-332853.1	16352247-3328525	UCL	3.397 ± 0.047^a	K4Ve	6	11.31	8.08	0.185	3.060	4330	0.94
163535.99-332634.7	16353598-3326347	UCL	3.169 ± 0.042	K3V	4	11.10	8.29	0.067	2.750	4550	1.02
153557.85-232404.3	15355780-2324046	US	0.803 ± 0.003	K3	11	12.37	9.43	0.222	2.750	4550	1.02
154106.78-265626.2	15410679-2656263	US	5.335 ± 0.123^a	K1V	6	11.22	8.92	0.000	2.295	4920	1.12
154249.91-253640.5	15424991-2536406	US	0.200 ± 0.001^b	G5	11	10.68	8.18	0.822	1.770	5500	1.24
154359.06-262251.1	15435905-2622516	US	3.744 ± 0.054	K9Ve	2	14.07	9.83	0.526	3.770	3880	0.69
154413.37-252258.7	15441334-2522590	US	6.406 ± 0.173	M1e	11	12.92	9.08	0.000	3.838	3630	0.50
154802.92-290837.0	15480291-2908369	US	2.188 ± 0.027^a	G9	10	10.90	8.62	0.195	2.100	5120	1.16
154812.03-234926.1	15481299-2349523	US	1.249 ± 0.009	M0.5Ve	2	13.97	9.27	0.681	4.090	3700	0.56
154821.29-244349.3	15482130-2443493	US	5.648 ± 0.154	G8	12	10.15	7.91	0.246	2.020	5210	1.18
154920.99-260006.2	15492100-2600062	US	1.994 ± 0.033^a	K4.5	13	11.18	7.91	0.063	3.210	4235	0.90
155145.36-245650.9	15514535-2456513	US	1.526 ± 0.012	K3IV	2	12.37	9.53	0.100	2.750	4550	1.02
155231.21-263352.6	15523122-2633529	US	3.300 ± 0.048^b	M0	10	12.78 ^c	8.98	0.000	3.804	3770	0.61
155403.59-292015.5	15540358-2920154	US	0.331 ± 0.001	M1.5	13	12.54	8.74	0.000	3.807	3560	0.45
155506.26-252110.2	15550624-2521102	US	3.592 ± 0.118	M1	10	12.33	8.51	0.000	3.815	3630	0.50
155655.47-225839.6	15565545-2258403	US	8.243 ± 0.269	M0.5	13	13.90	9.43	0.420	4.090	3700	0.56
155808.16-240552.6	15580815-2405529	US	0.506 ± 0.001	K4	10	12.23	8.96	0.226	3.060	4330	0.94
155812.70-232836.5	15581270-2328364	US	1.718 ± 0.025	G2IV	2	10.38	8.02	0.974	1.490	5870	1.31
155959.94-222036.9	15595995-2220367	US	0.862 ± 0.003	M1.0	13	13.24	8.63	0.435	4.220	3630	0.50
160000.77-250942.4	16000078-2509423	US	1.522 ± 0.012	G0	10	10.49	8.77	0.399	1.370	6050	1.34
160013.32-241810.4	16001330-2418106	US	4.384 ± 0.078	M0.5	13	13.61	9.51	0.012	4.090	3700	0.56
160040.55-220032.2	16004056-2200322	US	2.727 ± 0.035	G9	10	11.21	8.44	0.750	2.100	5120	1.16
160042.77-212737.9	16004277-2127380	US	0.579 ± 0.001^a	K7	10	12.76	8.92	0.249	3.620	3970	0.75
160147.43-204945.8	16014743-2049457	US	2.160 ± 0.022	M0	10	13.21	8.61	0.715	3.960	3770	0.61
160158.22-200812.0	16015822-2008121	US	1.774 ± 0.016^a	G9IV(e)	6	10.39	7.67	0.687	2.100	5120	1.16
160200.38-222123.7	16020039-2221237	US	2.876 ± 0.032^a	M1.0	13	13.58	8.84	0.577	4.220	3630	0.50
160208.46-225458.9	16020845-2254588	US	6.142 ± 0.148	M1.0	13	14.17 ^c	9.55	0.449	4.220	3630	0.50
160253.95-202248.1	16025396-2022480	US	1.954 ± 0.019^a	K7	10	12.44	8.19	0.708	3.620	3970	0.75
160311.83-323920.2	16031181-3239202	US	2.831 ± 0.029^a	K7	9	12.75	9.12	0.006	3.620	3970	0.75
160413.46-281037.5	16041346-2810378	US	0.806 ± 0.016^b	M1e	11	12.64	8.61	0.000	4.028	3630	0.50
160601.72-222653.3	16060171-2226534	US	0.978 ± 0.006	M0.5	14	12.50	8.46	0.000	4.049	3700	0.56
160654.36-241610.7	16065436-2416107	US	3.912 ± 0.170	M3e	11	12.72	8.86	0.000	3.861	3360	0.29

Table 2
(Continued)

1SWASP (J)	2MASS (J)	Subgroup	Period (days)	SpT	References	V (mag)	K_S (mag)	A_V (mag)	$(V - K_S)_0$ (mag)	T_{eff} (K)	M/M_{\odot}
160930.31-210458.8	16093030-2104589	US	8.196 ± 0.200	M0.0	13	12.77	8.92	0.000	3.856	3770	0.61
160939.70-220046.5	16093969-2200466	US	6.559 ± 0.488	K9IVe	2	13.99	9.30	1.029	3.770	3880	0.69
160940.98-221759.4	16094098-2217594	US	0.908 ± 0.011^b	M0e	11	12.53	8.44	0.143	3.960	3770	0.61
161028.87-221347.8	16102888-2213477	US	2.279 ± 0.034^a	G7IV(e)	6	9.84	7.23	0.746	1.950	5290	1.20
161042.01-210131.7	16104202-2101319	US	3.449 ± 0.115^a	K5e	11	12.33	8.56	0.468	3.350	4140	0.85
161156.34-230404.7	16115633-2304051	US	5.522 ± 0.350	M1e	11	13.04	8.82	0.003	4.220	3630	0.50
161302.72-225745.9	16130271-2257446	US	2.101 ± 0.030^a	K4	11	11.80	8.46	0.317	3.060	4330	0.94
161318.57-221249.0	16131858-2212489	US	5.885 ± 0.413^a	K1IV(e)	6	10.42	7.43	0.753	2.320	4920	1.12
161329.29-231107.4	16132929-2311075	US	3.114 ± 0.132^a	K1	11	11.74	8.49	1.038	2.320	4920	1.12
161400.35-210843.8	16140035-2108439	US	4.276 ± 0.264	K8IVe	2	13.74	9.60	0.528	3.670	3940	0.73
161402.12-230102.0	16140211-2301021	US	2.980 ± 0.053^a	G4	11	11.19	8.61	1.007	1.680	5620	1.26
161520.24-325504.9	16152023-3255051	US	5.728 ± 0.140^a	K5	9	11.99 ^c	8.56	0.092	3.350	4140	0.85
161535.86-252900.6	16153587-2529008	US	1.897 ± 0.021	K2.5IVE	2	12.43	8.74	1.195	2.620	4655	1.05
161557.03-324124.2	16155696-3241250	US	3.203 ± 0.042	K6	9	12.22 ^c	9.21	0.000	3.013	4020	0.78
161617.93-233947.5	16161795-2339476	US	2.620 ± 0.039^a	G9IV	6	10.63	8.10	0.476	2.100	5120	1.16
161731.38-230336.0	16173138-2303360	US	2.280 ± 0.044^a	K1.5	13	10.13	7.97	0.000	2.159	4840	1.10
161933.95-222829.4	16193396-2228294	US	4.067 ± 0.182^a	K1IV	6	11.45	8.51	0.693	2.320	4920	1.12
161950.57-335445.3	16195058-3354453	US	2.665 ± 0.031^a	G6V	6	10.20	8.41	0.000	1.788	5390	1.22
161950.73-215436.0	16195068-2154355	US	1.272 ± 0.013^a	K8IVe	2	12.50	8.20	0.700	3.670	3940	0.73
162029.25-325409.6	16202930-3254096	US	1.872 ± 0.014	K4IV(e)	2	12.26	8.99	0.233	3.060	4330	0.94
162905.84-314525.1	16290585-3145250	US	2.712 ± 0.040	K5IVe	2	12.52 ^c	9.09	0.086	3.350	4140	0.85

Notes. This table contains the members of Sco–Cen reported based on the criteria described in Section 3.1.2. Provided are cross-identifications of SWASPJ and 2MASSJ identifiers, periods and uncertainties, the spectral type and reference for the 157 stars with spectral types, APASS V magnitudes, 2MASS $V - K_S$ magnitudes, adopted reddening coefficients, T_{eff} , and mass.

^a Stars that have statistically similar periods to the nearest spatial entry in the Variable Star Index (Watson 2006).

^b Stars that have statistically different periods to the nearest spatial entry in the Variable Star Index (Watson 2006).

^c Stars without spectral types use the Sco–Cen subgroup-averaged reddening coefficients for color estimation only.

^d The only star in our sample found in David et al. (2014). We find the same period.

^e Stars for which the APASS V band was unavailable; SPM4 photometry was adopted in its place.

References. (1) Riaz et al. (2006); (2) Pecaut & Mamajek (2016); (3) Houk (1978); (4) Mamajek et al. (2002); (5) Spencer Jones & Jackson (1936); (6) Torres et al. (2006); (7) Houk (1982); (8) Wichmann et al. (1997); (9) Krautter et al. (1997); (10) Köhler et al. (2000); (11) Preibisch et al. (1998); (12) Houk & Smith-Moore (1988); (13) Rizzuto et al. (2015); and (14) Luhman & Mamajek (2012).

(This table is available in machine-readable form.)

Table 3
Data for Other Stars

Name	Group	1SWASP (J)	2MASS (J)	Period (days)	Spectral Types	References
CD-43 6891	...	111434.43-441824.1	11143442-4418240	0.973 ± 0.004 ^b	K2IV	5
CD-43 6891	...	111434.43-441824.1	11143442-4418240	39.92 ± 2.10 ^a	K2IV	5
TWA 12	TWA	112105.46-384516.5	11210549-3845163	3.311 ± 0.051 ^a	M1Ve	1
TWA 20	TWA	123138.06-455859.3	12313807-4558593	1.822 ± 0.014 ^a	M3IVe	5
RX J1539.7-3450	Lup I	153946.41-345102.2	15394637-3451027	7.127 ± 0.204 ^a	K4	2
HT Lup	Lup I	154512.86-341730.5	15451286-3417305	4.304 ± 0.109 ^a	K3Ve	1
HD 140655	Lup I	154558.54-341341.2	15455855-3413411	2.753 ± 0.035	F8V	3
RX J1546.8-3459	Lup I	154645.09-345947.3	15464506-3459473	2.278 ± 0.025	M0	2
RX J1548.1-3452	Lup I	154808.93-345253.2	15480893-3452531	1.423 ± 0.020	M2.5	2
RX J1548.9-3513	Lup I	154854.16-351318.5	15485411-3513186	0.933 ± 0.003	K6	2
IM Lup	Lup II	155609.20-375605.9	15560921-3756057	7.309 ± 0.183	M0	4
MML 78	Lup III	160545.00-390606.5	16054499-3906065	1.261 ± 0.007 ^a	G7V	5
RX J1607.2-3839	Lup III	160713.73-383923.3	16071370-3839238	2.418 ± 0.026	K7	2
IRAS 16051-3820	Lup III	160830.70-382826.8	16083070-3828268	6.244 ± 0.129	K0?	6
RX J1608.9-3905	Lup III	160854.27-390605.6	16085427-3906057	2.005 ± 0.028 ^a	K2	2
V1095 Sco	Lup III	160939.52-385506.8	16093953-3855070	2.912 ± 0.037 ^a	K5	2
Sz 122	Lup III	161016.43-390805.0	16101642-3908050	0.287 ± 0.001	M2e	4
RX J1612.0-3840	Lup III	161201.38-384027.5	16120140-3840276	2.813 ± 0.033 ^a	K5	2
RX J1620.7-2348	Oph	162045.96-234820.2	16204596-2348208	3.355 ± 0.139	K3e	7
RX J1621.0-2352	Oph	162057.86-235234.4	16205787-2352343	2.097 ± 0.046 ^a	G9IV	1
EM* StHa 126	Oph	162307.84-230059.8	16230783-2300596	4.069 ± 0.235 ^a	K2	7
EM* SR 6	Oph	162528.63-234626.1	16252863-2346265	3.760 ± 0.119	K2IV	5
CD-27 10938	Oph	162627.35-275651.0	16262736-2756508	2.065 ± 0.281 ^a	K4IVe	5
VSS II-28	Oph	162652.81-234312.6	16265280-2343127	5.595 ± 0.322 ^a	K1IVe	5
HBC 644	Oph	163104.44-240435.8	16310436-2404330	0.973 ± 0.019 ^b	K4IVe	5
V940 Sco	Oph	163201.59-253025.7	16320160-2530253	2.452 ± 0.035 ^a	K5IVe	5
V709 CrA	CrA	190134.84-370056.6	19013485-3700565	2.244 ± 0.021	K2.5	8
RX J1917.4-3756	CrA	191723.82-375650.3	19172382-3756504	3.375 ± 0.045 ^a	K0IVe	1

Notes.

^a Stars that have statistically similar periods to the nearest spatial entry in the Variable Star Index (Watson 2006).

^b Stars that have statistically different periods to the nearest spatial entry in the Variable Star Index (Watson 2006).

References. (1) Torres et al. (2006); (2) Krautter et al. (1997); (3) Houk (1982); (4) Hughes et al. (1994); (5) Pecaut & Mamajek (2016); (6) Antonucci et al. (2014); estimates $T_{\text{eff}} = 5000$ K, which would be roughly consistent with a K0 pre-MS star on the spectral type versus T_{eff} scale of Pecaut & Mamajek (2013); (7) Preibisch et al. (1998); (8) Meyer & Wilking (2009).

sample, the best spatial matches had poor brightness matches. The worst offenders revealed themselves as unphysical outliers on a color–magnitude diagram (V_J versus $V_{\text{APASS}} - K_s$). These cases were found to each be caused by two 2MASS targets of significant ($\gtrsim 0.75$ mag) brightness difference existing in close spatial proximity to a single SuperWASP target. Each was corrected by simply selecting the 2MASS counterpart as the one of (obvious) comparable brightness to the SuperWASP target.

Many smaller but significant ($0.2 \lesssim \Delta V \lesssim 0.75$ mag) brightness differences remained in cases with no spatial degeneracy of 2MASS counterparts. This prompted us to compare the SuperWASP and 2MASS brightnesses and positions with those of the APASS and SPM4 surveys as an additional check. The 2MASS, APASS, and SPM4 brightnesses were found to be in excellent agreement: e.g., $(\Delta V)_{\text{average}} \simeq 0.01$ mag for the APASS and SPM4 catalogs. However, the SuperWASP brightnesses were found to have much poorer agreement: e.g., $(\Delta V)_{\text{average}} \simeq 0.1$ mag when comparing the converted SuperWASP V magnitudes to either of the APASS or SPM4 catalogs, a factor of 10 worse. Figure 2 panel (a) shows the distribution of brightness differences between SuperWASP and APASS. The sizable skewing of SuperWASP data to brighter magnitudes can be attributed to blending due to SuperWASP’s large pixel scale. Panels (b), (c), and (d) show the J2000 positional differences between the four

surveys. While these differences are all small at $(\Delta r)_{\text{average}} < 0''.6$ or better, the APASS positions agree best with those of 2MASS at $(\Delta r)_{\text{average}} = 0''.12$.

APASS Johnson V -band magnitudes were used instead of the converted SuperWASP V magnitudes for all other aspects of our study (e.g., colors, reddening, HR diagram analysis). All of this gave us the highest confidence in the APASS V magnitudes and the lowest confidence in the SuperWASP V magnitudes. SPM4 Johnson V magnitudes were adopted only for the five stars in our 162 star sample for which APASS V magnitudes are not available. Finally, we computed $V - K_s$ colors for the stars in our sample using the adopted V magnitudes (from APASS or SPM4) and 2MASS K_s magnitudes. Figure 3 shows a de-reddened color–magnitude diagram for the final sample of 162 members of the three Sco–Cen subgroups. The treatment used for interstellar reddening and extinction is discussed later in Section 3.2.

3. Analysis

3.1. Time-series Analysis

3.1.1. Data Reduction

SuperWASP photometric data requires additional data reduction beyond its own pipelines (Collier Cameron et al. 2006).

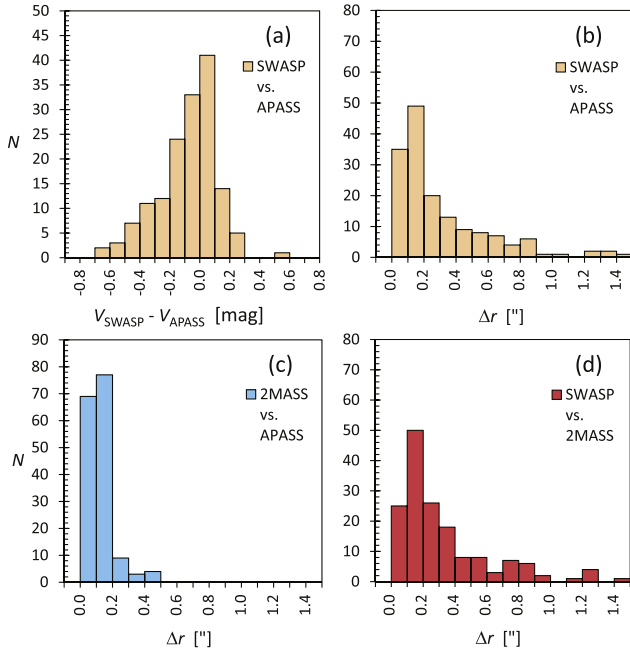


Figure 2. Select distributions of spatial and brightness differences between the SuperWASP, APASS, and 2MASS data sets for the final 162 star sample. In panel (a) the brightnesses for both surveys are in Johnson V magnitudes. The remaining panels show the J2000 positional differences.

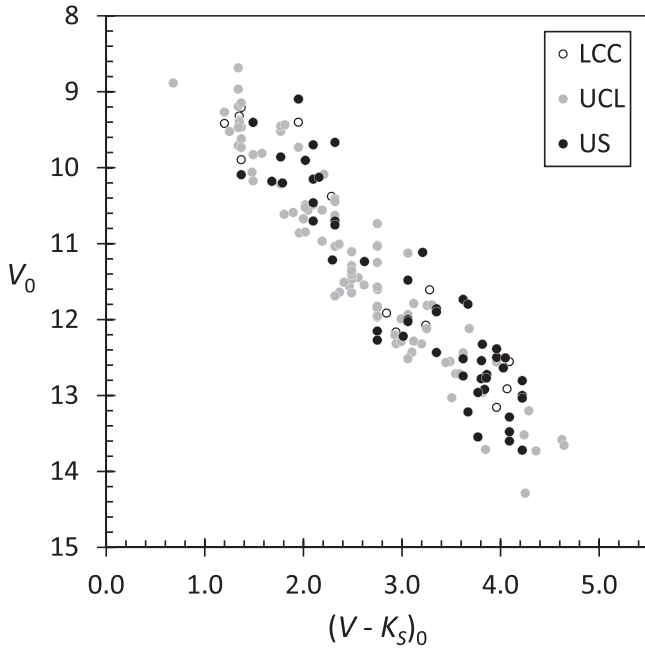


Figure 3. Dereddened color–magnitude diagram for the final sample of 162 stars in the classic Sco–Cen subgroups of US (filled black circles), UCL (filled gray circles), and LCC (open circles). The V -band brightness on both axes is APASS Johnson V , and the K_S value is from 2MASS.

Reported photometric errors, median binning, and a 3σ clip were used to further reduce the data. Data points with reported photometric errors of >0.1 mag were removed. Each data set was median combined and the standard error of the mean for each binned point was recorded; the low-period limit of 0.1 days was used because stars are not expected to have rotation periods shorter than this due to instability (Hartman et al. 2010).

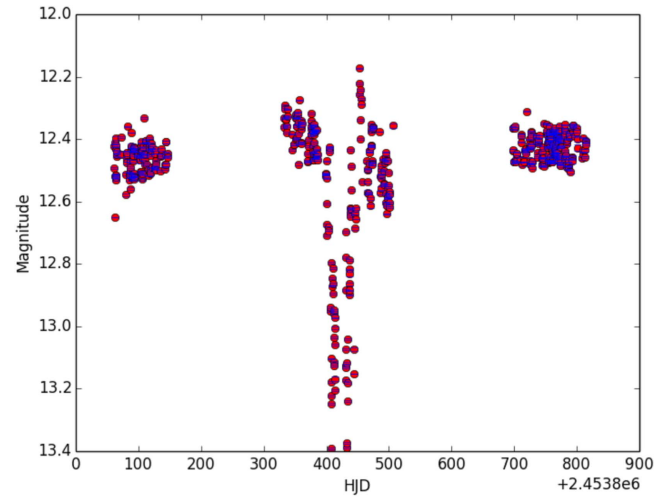


Figure 4. Reduced SuperWASP light curve for J1407 over three observing seasons. Error bars (blue) are smaller than the data points themselves. The eclipse first detected by Mamajek et al. (2012) is clearly detected.

Bins with fewer than three points were removed. A 3σ clip was applied to the binned data to remove any remaining spurious points. The reduced data was separated into three individual ~ 100 day time frames (seasons). Finally, a plot of the full light curve, with error bars, was generated (Figure 4).

3.1.2. Periodograms

A custom periodogram analysis pipeline was written using the Python⁷ language. Modules from the SciPy⁸ stack: *scipy*, *numpy*, *matplotlib*, and *pandas* (Jones et al. 2001; Hunter 2007; McKinney 2010; Stéfan van der Walt & Varoquaux 2011) were used for reducing and plotting data (with error bars) (Section 3.1.1), performing Lomb-Scargle (LS) periodograms and generating phase-folded light curves with fitted amplitudes.

The LS periodogram (Press et al. 1992; Scargle 1982) is a powerful tool for extracting periods from unevenly sampled time-series photometry data sets (e.g., Hartman et al. 2008, 2010; Messina et al. 2010). The LS periodogram routine from the Python *scipy* module was applied to each observing season for each star. The period range spans from 0.1 days (see Section 3.1.1) to τ days with a period step size of 0.15 days where τ is the length of time for the data collected in a particular season. Periods corresponding to half the time length of the data set (τ) were searched to ensure that all possible long-term periods in the data set can be detected. The period step size provided a resolution in the periodogram fine enough to detect strong periods accurately over a large period span without being overly computationally expensive. After sorting data points into their individual seasons, the routine returned the normalized values, which were then plotted versus frequency.

We report the strongest period from each star’s periodogram in Table 1. The LS periodogram routine alone does not estimate false positive periods, so the method of Cargile et al. (2014) was employed to calculate false alarm probabilities (FAPs). In the interest of computational time, FAPs were only calculated for our final 162 star sample (Table 2) and the 27 “other” stars (Table 3).

⁷ <http://python.org>

⁸ <http://www.scipy.org/>

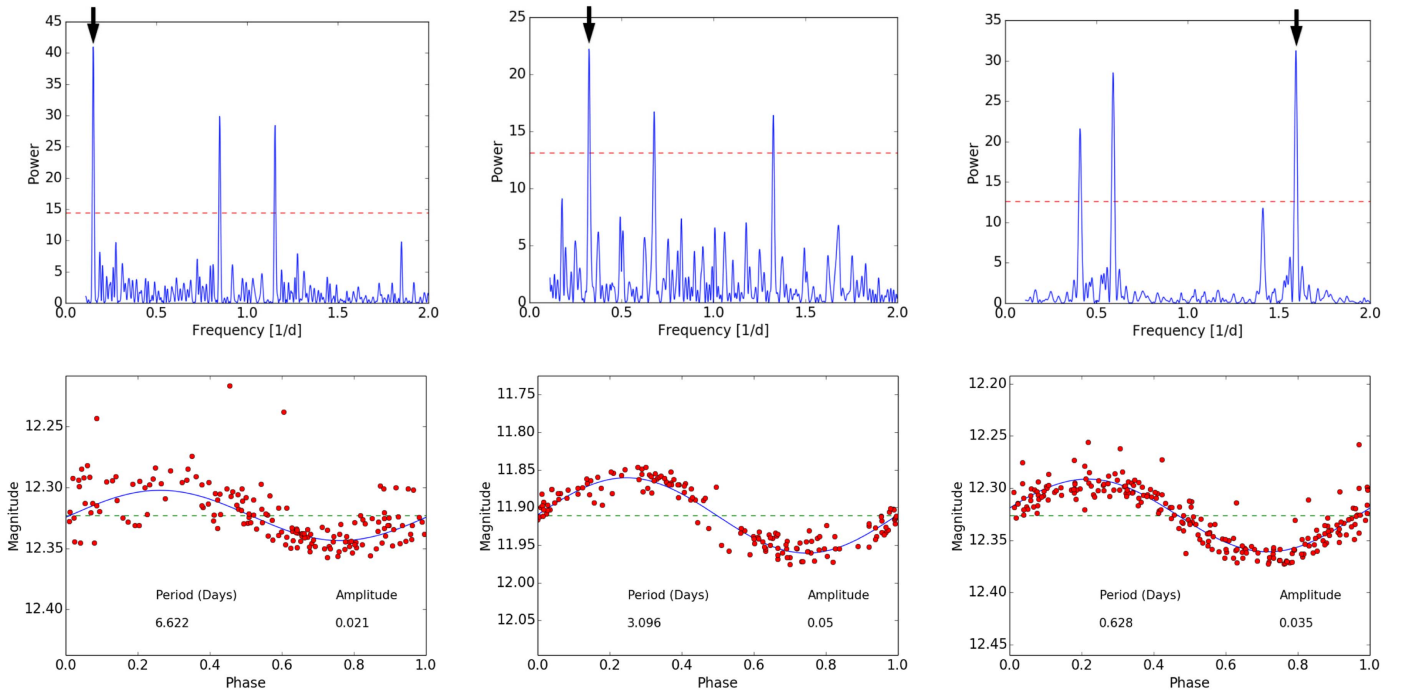


Figure 5. Periodograms (top figures) and phase-folded light curves (bottom figures) for three stars, illustrating a range of periods and amplitudes. The dashed red line represents the power at the 0.01 FAP, and the adopted frequencies for each star are marked with a black arrow. In the light curves, the best-fit sinusoid is plotted in blue and the green dashed line represents the SWASP mean magnitude. Left: 2MASS J15082502-3337554, Center: 2MASS J13191370-4506326, Right: 2MASS J11132622-4523427.

In short, the FAP for a given star was estimated by randomly shuffling its light curves photometric values relative to its time values (after binning), creating a new, randomized light curve. Next, a periodogram was created for this randomized light curve and its strongest period saved. This was repeated 10^4 times, and the resulting strongest periods were plotted as a histogram. Finally, the strongest period from the real light curve was compared to this histogram. The period was considered to be a real detection only if less than 10% of the histograms periods had stronger peaks. In this case, we say the $FAP < 0.01$. Obvious aliases (periods occurring at integer multiples of the strongest period) were vetted by eye. Figure 5 shows three example light curves with their corresponding periodograms and FAP levels. The uncertainties for the periods were measured only for the stars presented in Tables 2 and 3. The maximum peak in the periodogram for each season was fit with a Gaussian using a least-squares routine. The means and variances were averaged for each season and reported in Tables 2 and 3. The light curves for each star were then phase-folded over its seasonal period and plotted. Using the *scipy* least-squares fitting tool, a sine curve is fit to each phase-folded light curve (Figure 5).

Figure 5 contains example periodograms and light curves for three example stars in our sample. The criteria for a detected rotation period are (1) a periodogram peak must be above the 0.01 FAP plot threshold, (2) that said peak is consistent through at least two seasons of SuperWASP data, and (3) a consistent light curve amplitude (to within a few 0.1 mag) through at least two seasons. Furthermore, the stars reported must be confirmed members of Sco-Cen (see Section 2.2.1). In order to completely profile each star and compare them to angular momentum evolution models (see Figures 7 and 8), the star must have a published spectral type and be a member of one of the three main subgroups.

3.2. Intrinsic Color, Temperature, and Mass Modeling

To investigate the angular momentum evolution of Sco-Cen stars, it is constructive to plot the rotation periods determined from the periodogram analysis as a function of intrinsic stellar properties. In particular, the measured spectral types for 157 stars in our sample enabled us to estimate intrinsic colors ($V - K_s$), effective temperatures (T_{eff}), and masses (M). The intrinsic $V - K_s$ and T_{eff} were determined from the empirical relations and BT-Settl grid models, respectively, from Table 6 of Pecaut & Mamajek (2013). Based on these T_{eff} values, we computed M using the theoretical isochrones of (Baraffe et al. 2015, hereafter BHAC15; adopting the mean age of each star's subgroup):

$$\begin{aligned} \log(M/M_{\odot}^N) = & -(3.5075918704 \times 10^4) \\ & + (3.7421144677 \times 10^4) \cdot \log(T) \\ & - (1.4972186556 \times 10^4) \cdot \log(T)^2 \\ & + (2.6625089056 \times 10^3) \cdot \log(T)^3 \\ & - (1.7755725859 \times 10^2) \cdot \log(T)^4, \quad (3) \end{aligned}$$

this is valid over the range of $3056 \text{ K} < T_{\text{eff}} < 6422 \text{ K}$ and $0.1 < M/M_{\odot}^N < 1.4$, and has a calibration uncertainty of approximately $\sigma(\log(M/M_{\odot}^N)) \simeq 0.007 \text{ dex}$. Table 2 lists the intrinsic $V - K_s$, T_{eff} , and masses determined for the stars in our sample, and period-color, period-temperature, and period-mass diagrams are plotted in Figure 6.

Interstellar reddening was estimated using $B - V$, $V - J$, $V - H$ and $V - K_s$. The observed colors were computed from BV photometry collected from various sources (e.g., APASS DR9, *Hipparcos*, Tycho-2, or other ground-based photometry) and near-infrared photometry from 2MASS (Cutri et al. 2003a). The photometry adopted for estimating extinctions is listed in

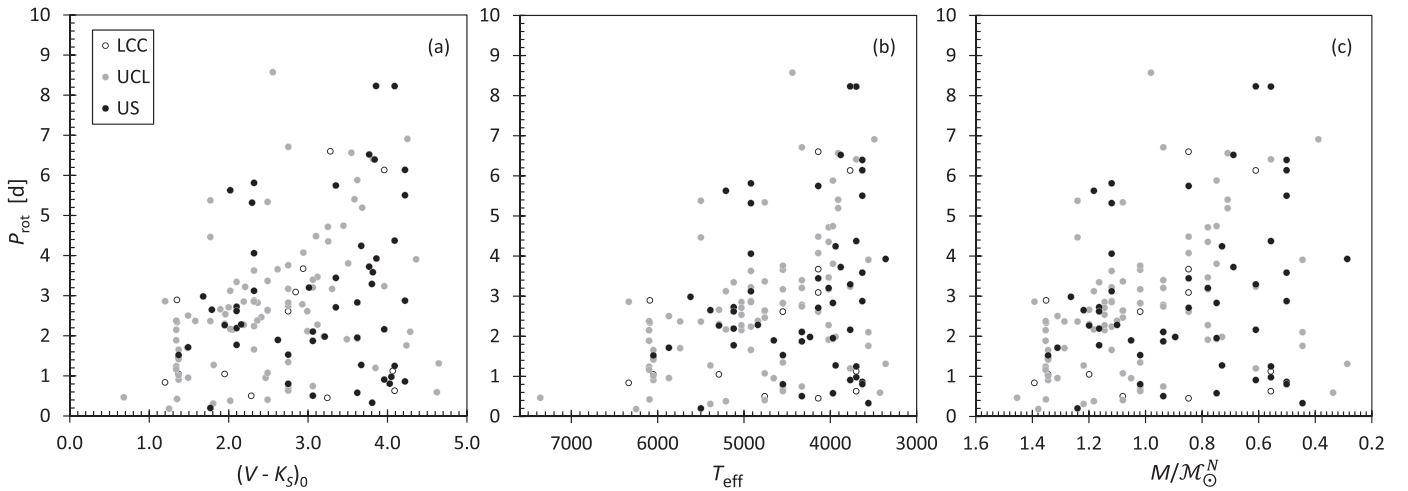


Figure 6. Period–color, –temperature, and –mass diagrams. The vertical axes plot the season-averaged rotation period determined from the SuperWASP periodogram analysis in units of days, P_{rot} . The horizontal axes plot the extinction-corrected observed color $V - K_s$ in magnitudes (Panel a), the modeled effective temperature T_{eff} in units of K (Panel b), and the modeled mass in units of solar masses, M/M_{\odot}^N (Panel c). Panel (a) contains the complete final sample of 162 stars in the classic Sco–Cen subgroups of US (filled black circles), UCL (filled gray circles), and LCC (open circles), whereas panels (b) and (c) contain only the 157 of these stars with measured spectral types—since the temperature and mass models depend on the spectral type.

Table 4
Adopted Photometry for Stellar Parameters

2MASS (J)	B (mag)	References	V (mag)	References	J (mag)	H (mag)	K_S (mag)
11132622-4523427	14.370 ± 0.012	DR9	12.833 ± 0.010	DR9	9.415 ± 0.028	8.727 ± 0.040	8.495 ± 0.031
12441932-4525235	10.087 ± 0.035	H00	9.500 ± 0.022	H00	8.371 ± 0.027	8.072 ± 0.047	7.999 ± 0.033
12480778-4439167	10.650 ± 0.014	T06	9.830 ± 0.010	T06	8.131 ± 0.021	7.672 ± 0.055	7.513 ± 0.024
12543141-4607361	10.250 ± 0.038	H00	9.713 ± 0.024	H00	8.376 ± 0.029	7.983 ± 0.024	7.910 ± 0.023

Note. A sample of the adopted photometry for the stars with spectral types. The remainder of this table is available electronically. AAVSO Photometric All-Sky Survey (APASS) DR6, DR7 photometry retrieved from <https://www.aavso.org/download-apass-data>; Henden et al. (2016).

References. (DR6) APASS DR6; (DR7) APASS DR7; (DR9) APASS DR9; (P97) *Hipparcos*, Perryman et al. (1997); (H00) Converted from Tycho-2 B_T , V_T , H_{og} et al. (2000); (T06) Torres et al. (2006).

(This table is available in its entirety in machine-readable form.)

Table 4. The observed photometry was then compared to intrinsic color sequences for pre-MS stars as a function of spectral type from Pecaut & Mamajek (2013) to estimate color excesses $E(B - V)$, $E(V - J)$, $E(V - H)$, and $E(V - K_S)$. Extinctions for individual objects were computed using these four color excesses, as described in Pecaut & Mamajek (2016). The computed extinctions for each star are listed in Table 2.

For stars without a measured spectral type, the color excess and extinction coefficient were taken as the average of the other stars in the same subgroup: $E(V - K_S)_{\text{avg}} = 0.332$ for US and 0.173 for each of UCL and LCC; $(A_V)_{\text{avg}} = 0.372$ for US and 0.194 for each of UCL and LCC. These mean color excesses and extinctions were used to correct the observed V and $V - K_S$ values in the color–magnitude diagram of Figure 3 and the observed $V - K_S$ colors in the period–color plot of Figure 6 Panel (a).

4. Discussion

4.1. Results

Table 2 summarizes the relevant stellar parameters for our sample stars, including SWASP–2MASS cross-identifications, Sco–Cen subgroup assignments, season-averaged rotation periods, spectral types, colors, extinctions, effective temperatures, and estimated masses. A search of the literature found

only one variability study of stars across Sco–Cen with which to compare (David et al. 2014). We find that the only star with a reported period in both our survey and David et al. (2014) was HD 141277 (2MASS J15494499-3925089), with both surveys reporting the same rotation period of ~ 2.23 days. We queried the AAVSO International Variable Star Index (VSX) catalog via Vizieur using the 2MASS positions of our stars, with a $5''$ search radius; the search uncovered the nearest spatial matches (most $< 1''$ away) for 94 of our stars (Watson 2006). Of these 94 stars, 76 have periods similar to ours. There are 96 new rotation period measurements, including a second, shorter activity period measured for the Li-rich K giant CD-43 6891.

4.2. Rotational Evolution

For each star, we adopt the mean age of its subgroup and use its spectral type (and corresponding T_{eff}) to estimate a mass using isochrones (see Section 3.2). Figure 7 is a mass–period diagram for Sco–Cen with rotational evolution tracks from Gallet & Bouvier (2015) overplotted for several rotation rates at the ages of each major subgroup. In addition, a quadratic is plotted in an attempt visualize the rotational evolution trend of the ~ 11 – 17 Myr sample of pre-MS stars. The season-averaged rotation periods versus the age of each subgroup are plotted in Figure 8. The Gallet & Bouvier (2015) rotational evolution

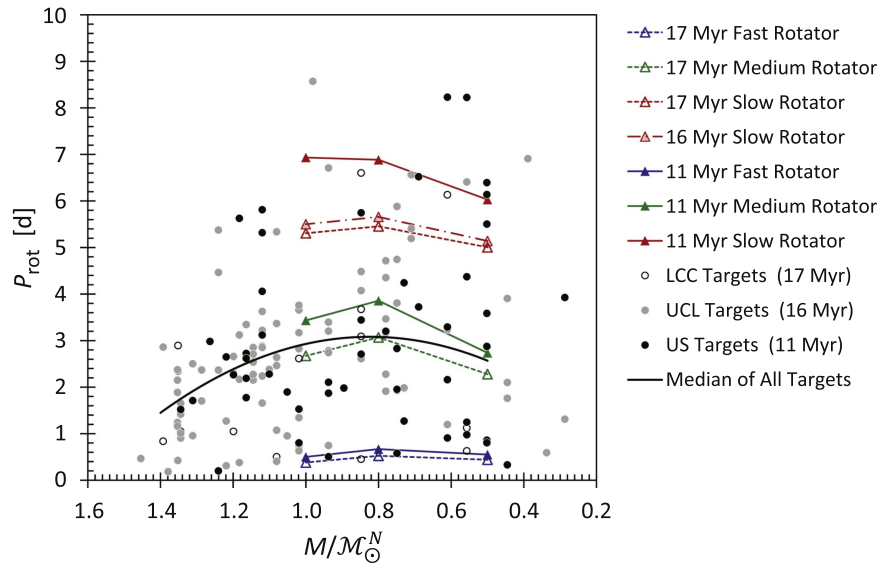


Figure 7. Period–mass diagram of Figure 6 panel (c) overlaid with the angular momentum evolutionary model tracks of Gallet & Bouvier (2015). As in Gallet & Bouvier (2015), tracks are shown for each of the “slow,” “medium,” and “fast,” rotators corresponding to the 25th, 50th, and 90th percentiles in rotational period of the stellar envelope. The modeled points (triangles) have been averaged by mass in bins of 0.4–0.6, 0.7–0.9, and 0.9–1.1 \mathcal{M}_{\odot}^N and are plotted at the mass bin centers; the connecting lines serve only to interpolate between these modeled points and do not themselves represent model data. Here only model tracks corresponding to the median ages of US, UCL, and LCC of 11, 16, and 17 Myr, respectively, are reproduced. Model tracks for the 16 Myr medium and fast rotators have been omitted since they are nearly identical to (i.e., overlap) those of the 17 Myr medium and fast rotators, respectively. For general comparison to the model tracks, a second-order polynomial (black solid line) was fit to the median periods of the 157 stellar data points (circles) in the same three mass bins as the models plus two additional bins of 1.1–1.3 and 1.3–1.5 \mathcal{M}_{\odot}^N .

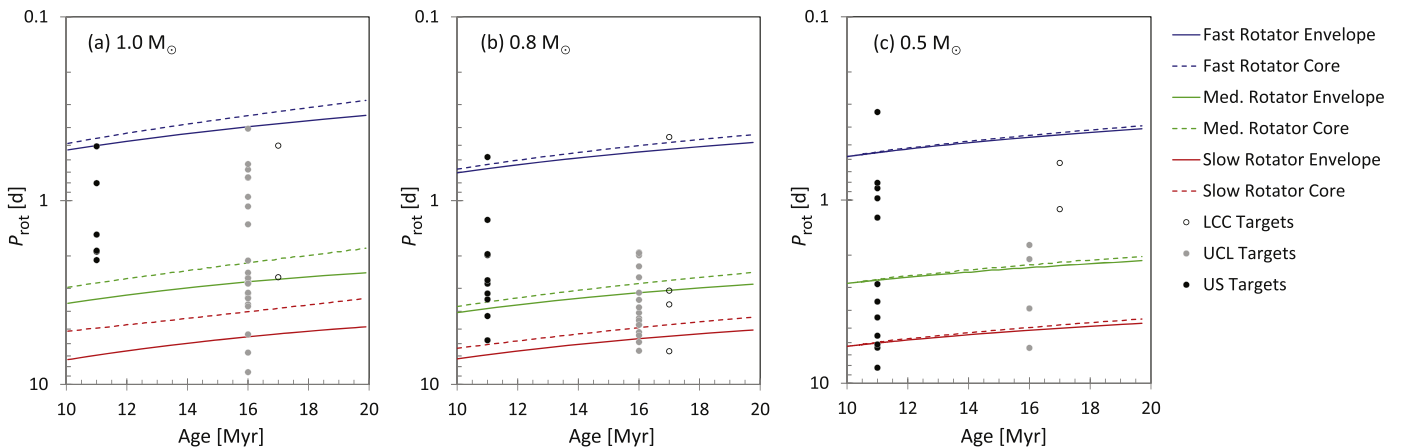


Figure 8. Reproduction of the period–age diagrams of Gallet & Bouvier (2015), Figure 5, with Sco–Cen stars from the present study (circles) overlotted. As in Gallet & Bouvier (2015), angular momentum evolutionary model tracks are shown for each of the “slow,” “medium,” and “fast,” rotators corresponding to the 25th, 50th, and 90th percentiles in rotational period for each of the stellar core and envelope. The modeled data are also averaged by mass in bins of 0.4–0.6 \mathcal{M}_{\odot}^N (panel a), 0.7–0.9 \mathcal{M}_{\odot}^N (panel b), and 0.9–1.1 \mathcal{M}_{\odot}^N (panel c). Only 82 stars of the final 162 star sample are shown since 5 do not have mass determinations and the rest have masses falling outside of these three mass ranges.

tracks are overplotted for different stellar masses and initial conditions (fast, medium, slow rotators); initial conditions were chosen to best match rotation period distributions of older and younger clusters. Our data show that the general trend in period and mass predicted by the Gallet & Bouvier (2015) models continue to do a reasonable job matching the Sco–Cen stars. The envelope of the fastest rotators in Sco–Cen between ~ 0.5 – $1 \mathcal{M}_{\odot}^N$ follows the fast rotator trend predicted by Gallet & Bouvier (2015). We show a few stars with periods of ~ 8 days that are rotating slightly slower than the envelope of the slowest rotators predicted by the Gallet & Bouvier (2015) models. All of our ~ 1.25 – $1.5 \mathcal{M}_{\odot}^N$ stars are rotating very fast (0.2–3 days)

and just below $\sim 1.25 \mathcal{M}_{\odot}^N$ stars are found with much slower rotation periods of ~ 5 –6 days.

These results suggest that while the stars that will eventually be early F dwarfs on the main sequence (FIV–F6V; 1.25 – $1.5 \mathcal{M}_{\odot}^N$) have rotation periods at ~ 11 – 17 Myr that, on average, are only slightly less than their G-type brethren (~ 2 days versus ~ 3 days, on average), the F-dwarf population appears to arrive on the main sequence with a population near breakup velocity ($P \simeq 0.2$ day; e.g., 1SWASP J154610.69–384630.2, 1SWASP J144619.03–354146.5), but lacking a population of slow rotators ($P > 3$ days). The early F-type stars remain fast-rotating throughout their main-sequence lifetimes, experiencing

only weak magnetic braking due to their weaker magnetic dynamos (e.g., Slettebak 1955; Kraft 1967).

4.3. Search for Eclipsing Systems

In addition to our rotation evolution study, this analysis included a search for any signatures of circumsecondary disks similar to 1SWASP J140747.93-394542.6 (J1407 = V1400 Cen; Mamajek et al. 2012; Scott et al. 2014). The asymmetric light curves of the stars ϵ Aurigae (Guinan & Dewarf 2002), EE Cep (Mikolajewski & Graczyk 1999), and J1407 are signatures of disk or ring systems occulting their host stars. These asymmetric eclipses are characterized by their long duration and magnitude-scale depths (e.g., EE Cep with a ~ 30 –90 day eclipse and depth of >2 mag; Mikolajewski & Graczyk 1999). An effective large-scale search for these eclipses (as proposed by Mamajek et al. 2012) would require a long-term (10 year), high-cadence time-series photometric survey of 10^4 post-accretion pre-MS stars—yielding only a few candidates.

All of the light curves from this analysis were scanned by eye for obvious eclipses, like J1407 (see Figure 4). To see an eclipse occur, it would have to be restricted to one of these 100 day windows (J1407 has a ~ 58 day eclipse duration; Mamajek et al. 2012). Additionally, the rotation period amplitudes vary on the 0.01 mag level (see Table 1). Thus, any amplitude variations on the 0.1 mag level would be evident in our periodogram search, making shorter-term <10 day eclipses evident. Therefore, no eclipses with durations of <100 days and depths >0.1 mag were detected in this sample.

This survey also uncovered five candidates for pre-MS eclipsing binaries (Figure 9). However, after further review of their astrometric data, we reject Sco–Cen membership for four of them. We argue that one of them (V2394 Oph) appears to be a poorly characterized, heavily reddened ($A_V \simeq 5$ mag) massive eclipsing binary in the LDN 1689 dark cloud of the Ophiuchus star-forming region of Sco–Cen. Further discussion on these eclipsing binaries can be found in the Appendix, and their phase-folded light curves are plotted in Figure 9.

4.4. Conclusion

This survey searched the SuperWASP archive for Sco–Cen members with measurable rotation periods and significant eclipsing events. A total of 189 reliable rotation periods were extracted—162 for stars in the classic Sco–Cen subgroups of US, UCL, and LCC, and 27 for stars in younger star-forming regions within the Sco–Cen complex. Of these, 157 of the classic subgroup members have previously reported spectral types. These spectral types were used to estimate masses to compare our data against current angular momentum evolution models from Gallet & Bouvier (2015), and the rotation periods appear to be in reasonable agreement with the range of periods predicted by the models. No new eclipsing circumsecondary disks were detected beyond the previously known V1400 Cen (J1407) system. Five eclipsing binary systems were identified, but only one appears to be a strong candidate for membership in Sco–Cen (V2394 Oph in the LDN 1689 dark cloud in Ophiuchus). The remaining four eclipsing binaries all appear to be interlopers.

S.N.M. was supported by NSF award PHY-1156339 for the University of Rochester REU program. E.E.M. acknowledges support from NSF award AST-1313029. S.N.M. and E.E.M.

also acknowledge support from the NASA NExSS program. This work used the VizieR and SIMBAD services. Part of this research was carried out at the Jet Propulsion Laboratory, California Institute of Technology, under a contract with the National Aeronautics and Space Administration. We also acknowledge and thank Florian Gallet for providing the angular momentum evolution tracks used to generate Figures 7 and 8. This paper makes use of data from the first public release of the WASP data (Butters et al. 2010) as provided by the WASP consortium and services at the NASA Exoplanet Archive, which is operated by the California Institute of Technology, under contract with the National Aeronautics and Space Administration under the Exoplanet Exploration Program. This paper has been approved for Unlimited External Release by JPL (URS 264518).

Appendix A

Periods for Other Stars in Sco–Cen Complex

SuperWASP time-series photometry was found for 27 other stars. These stars are associated with neighboring subgroups (some of which are active star-forming regions, e.g., Lup, Oph, CrA), i.e., their positions and/or kinematics are inconsistent with membership within the three classic older subgroups (LCC, UCL, US). Two are associated with the TWA Hya group. We also found a Li-rich K giant with two measured periods, which is elaborated on later in the Appendix. Their estimated rotation periods (calculated following the analysis in Section 3), along with their 2MASS alias and spectral type are presented in Table 3.

Appendix B

A Massive Eclipsing Binary in Ophiuchus: V2394 Oph

1SWASP J163140.67-242516.2 (V2394 Oph, TYC 6799-309-1, CoD-24 12698) is a 0.59 day eclipsing binary whose components are probably either in contact or close. The star is situated in the LDN 1689 cloud (Nutter et al. 1833), and has been previously selected as a proper motion member of either Upper Sco (Hoogerwerf et al. 2000) and/or Oph (Makarov 2007). A very strong period of 0.295 day is clearly detected in all three seasons of SuperWASP data. Phase-folded time-series photometry at 0.295 day suggests that the secondary eclipse depth is ~ 0.2 mag and the primary eclipse depth is ~ 0.4 mag. The long-term out-of-eclipse brightness seems to be varying at the ~ 0.1 mag level over the three years. Grankin et al. (1996) report the eclipsing binary to have photometry at maximum of $V = 10.01$, $U - B = 0.40$, $B - V = 0.95$. Barnard (1910) and Struve & Straka (1962) both commented on the concentration of nebulosity centered on the star (called CD $-24^\circ 12684$ in these publications), and Struve & Straka (1962) comments on a very red reflection nebula surrounding the star and reports that a spectrum taken by George Herbig in 1949 revealed the star to be A0 or A1. Vrba et al. (1976) reported the star (VSS II-50) as spectral type B9, and estimated the star to have extinction $A_V \simeq 3.29$ ($E(B - V) = 1.06$). The Grankin et al. (1996) colors at maximum light are a good match to a $T_{\text{eff}} \simeq 9700$ K dwarf with $E(B - V) = 1.47$ ($A_V = 4.87$ mag), which would be consistent with $\sim A0$ type.

Is this star associated with Sco–Cen? The *Gaia* DR1 TGAS astrometry for star lists proper motion $\mu_\alpha, \mu_\delta = -6.672, -24.594$ ($\pm 1.599, \pm 1.803$) mas yr^{-1} and parallax $\varpi = 7.23 \pm 0.58$ mas (consistent with distance 138 ± 11 pc). The proper motion is similar to the mean proper motion of the YSOs in the

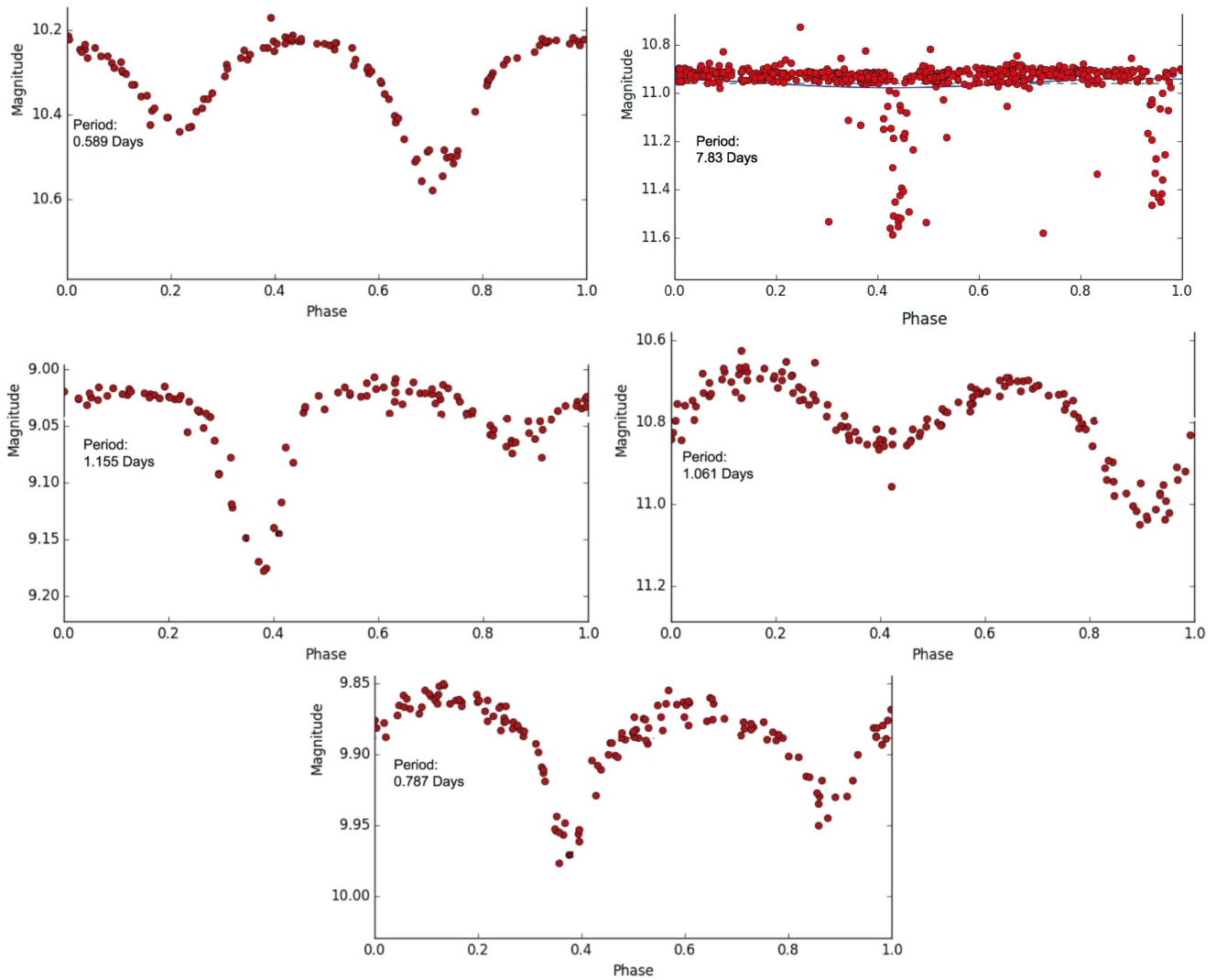


Figure 9. Phase-folded light curves for our five eclipsing binary detections (all season 1 detections). Top Left: TYC 6799-309-1, Top Right: TYC 7807-358-1, Middle Left: HD 134518, Middle Right: TYC 7322-822-1, Bottom: TYC 7340-720-1.

Oph embedded cluster: $\mu_\alpha, \mu_\delta = -10, -27 (\pm 2, \pm 2)$ mas yr⁻¹ (Mamajek 2008). The mean distance to the Oph cluster has been estimated recently to be 131 ± 3 pc (Mamajek & Hillenbrand 2008), 119 ± 6 pc (Lombardi et al. 2008), $120.0^{+4.5}_{-4.2}$ pc (Loinard et al. 2008), but a recent VLBA trigonometric parallax survey of 16 systems by Ortiz-León et al. (2017) refined the mean distance to 137.3 ± 1.2 pc. Hence, both the *Gaia* DR1 TGAS proper motion and parallax are statistically consistent with the rest of the YSO population in the Oph cloud. If the star is associated with Oph, its radial velocity is predicted to be -6.5 km s⁻¹. The star is in very close proximity with four other lower-mass YSOs within 3' (~ 0.12 pc projected radius; DoAr 43, 44, 46, and 2MASS J16313124-2426281), which may consist of an unstable dynamical trapezium.

Hence, V2394 Oph appears to be not only comoving with Upper Sco and Oph, in the immediate vicinity of other YSOs, associated with nebulosity, and a *Gaia* DR1 parallax consistent with being co-distant with the Oph clouds (see clumping of parallaxes for stars illuminating reflection nebulae in Mamajek & Hillenbrand 2008). The photometry is consistent with an unresolved, unextincted V_o magnitude of 5.14. Using the TGAS parallax, we estimate an unresolved absolute magnitude of $M_V = -0.6$, which places it about 2 mag above the zero-age

main sequence (Aller et al. 1982). Through comparison with the Siess et al. (2000) isochrones, and considering the unknown mass and radii ratios of the components, we propose that the V2364 Oph system is a ~ 1 – 2 Myr-old contact or near-contact eclipsing binary where the primary is a ~ 3 – $5 M_\odot$ star. Erickson et al. (2011) only identify four members of the Oph clouds whose spectral types are A0 or earlier (HD 147889, SR 3, Oph S1, WLY 2-48), and now V2394 Oph appears to be the most massive member specifically of the LDN 1689 dark cloud.

Appendix C Other Eclipsing Binaries

ISWASP J140807.34-393548.8 (TYC 7807-358-1, ASAS J140807-3935.9, CD-39 8717) appears to be a 7.815 day eclipsing binary with primary eclipse depth of ~ 0.7 mag and secondary eclipse depth of ~ 0.6 mag. The strongest peaks have periods of 7.83 days (the season 1 phase-folded light curve shows two minima), 3.91 days (the season 2 single minimum), and 3.895 days (the season 3 single minimum with large scatter). This star was selected as a candidate UCL member by virtue of its proper motion by Hoogerwerf et al. (2000). The

UCAC4 proper motion is suggestive of LCC membership; however, the kinematic parallax ($\varpi = 9.30 \pm 0.62$ mas) we calculate using the UCAC4 proper motion and LCC space motion from Chen et al. (2011) differs from the *Gaia* DR1 parallax ($\varpi = 2.98 \pm 0.75$ mas) by 6.5σ . We conclude that this is a background interloper unrelated to Sco–Cen.

ISWASP J151126.76-361457.2 (HD 134518) is a 1.154 day eclipsing binary with a primary eclipse depth of ~ 0.15 mag and secondary eclipse depth of ~ 0.05 mag. Very strong peaks at exactly 0.577 days are detected in each of the three seasons. This star was mentioned as a UCL candidate by de Geus et al. (1989). Perevozkina & Svechnikov (2004) classifies the system as A7+[K5], and Houk (1982) classifies the blended spectrum as A8V. The revised *Hipparcos* parallax ($\varpi = 7.72 \pm 1.81$ mas van Leeuwen 2007) and light estimated reddening ($E(B-V) \simeq 0.09$) are both similar to other UCL members (mean $\varpi \simeq 7.1$ mas); however, the revised *Hipparcos* proper motion is off of the mean UCL motion (Chen et al. 2011) by $\sim 5 \text{ km s}^{-1}$ —much larger than the 1D velocity dispersion of the group ($\sim 1.3 \text{ km s}^{-1}$). The *Hipparcos* parallax translates the primary’s HRD position to on the main sequence and below the trend for other Sco–Cen members. We consider HD 134518’s membership to UCL unlikely, but further follow-up is warranted. If HD 134518 belongs to UCL, its systemic radial velocity should be 3 km s^{-1} .

ISWASP J153554.13-335623.6 (TYC 7322-822-1) is a 1.06 day eclipsing binary showing a primary eclipse depth of ~ 0.3 mag and secondary eclipse depth of ~ 0.2 mag. The system showed very clean 0.53 day peaks in all three seasons. Hoogerwerf et al. (2000) selected the star as a candidate UCL member based on its proper motion. The star’s *Gaia* DR1 parallax ($\varpi = 3.19 \pm 0.78$ mas) differs from the kinematic parallax we calculate ($\varpi = 8.52 \pm 0.70$ mas; adopting its UCAC4 proper motion and assuming UCL space velocity from Chen et al. 2011) by 5.1σ . We conclude that this is a background interloper.

ISWASP J154856.93-363920.2 (TYC 7340-720-1) is a 0.393 day contact binary with primary eclipse depth of ~ 0.10 mag and secondary eclipse depth of ~ 0.08 mag. Hoogerwerf et al. (2000) selected this star as a candidate UCL member based on its proper motion. The *Gaia* DR1 parallax ($\varpi = 6.51 \pm 0.32$ mas) is similar to other UCL members; however, the *Gaia* TGAS proper motion is off of the predicted UCL motion by $8 \pm 1 \text{ mas yr}^{-1}$ ($7 \pm 1 \text{ km s}^{-1}$). We conclude that the star is an interloper.

Appendix D

A Li-rich Red Giant Interloper

ISWASP J111434.43-441824.1 (2MASS J11143442-4418240, CD-43 6891) gave conflicting signals regarding its potential Sco–Cen membership. The star was found by Pecaut & Mamajek (2016) to be a Li-rich ($\text{EW}(\text{Li I } \lambda 6707) = 670 \text{ m}\text{\AA}$) X-ray-emitting K2IV star; however, its inferred isochronal age (1 Myr) appeared to be extraordinarily young. The star has a large photometric amplitude (~ 0.2 mag) and long period (37 day), for which Richards et al. (2012) classified its light curve as that of a small-amplitude red giant type B. Both Rybka (2007) and Gontcharov (2008) flag the star as being a likely clump red giant. The new *Gaia* DR1 parallax ($\varpi = 2.18 \pm 0.25$ mas; *Gaia* Collaboration et al. 2016) is clearly at odds with the predicted kinematic parallax calculated by Pecaut & Mamajek (2016; $\varpi = 6.56 \pm 0.60$ mas; which assumed Sco–Cen

membership). Ignoring the effects of extinction, this translates to an absolute magnitude of $M_V \simeq 1.5$, which puts it squarely among other K2 giants. We conclude that the star is a rare Li-rich giant, and an interloper.

References

- Aller, L. H., Appenzeller, I., Baschek, B., et al. 1982, in Landolt–Börnstein: Numerical Data and Functional Relationships in Science and Technology—New Series (Berlin: Springer), 54
- Antoniucci, S., García López, R., Nisini, B., et al. 2014, *A&A*, 572, A62
- Ardila, D., Martín, E., & Basri, G. 2000, *AJ*, 120, 479
- Baraffe, I., Homeier, D., Allard, F., & Chabrier, G. 2015, *A&A*, 577, A42
- Barnard, E. E. 1910, *ApJ*, 31, 8
- Barnes, S. A. 2010, *ApJ*, 722, 222
- Blaauw, A. 1946, *PGro*, 52, 1
- Bouvier, J., Matt, S. P., Mohanty, S., et al. 2014, in Protostars and Planets VI, ed. H. Beuther, R. S. Klessen, C. P. Dullemond, & T. Henning (Tucson, AZ: Univ. of Arizona Press), 433
- Butters, O. W., West, R. G., Anderson, D. R., et al. 2010, *A&A*, 520, L10
- Cargile, P. A., James, D. J., Pepper, J., et al. 2014, *ApJ*, 782, 29
- Chen, C. H., Mamajek, E. E., Bitner, M. A., et al. 2011, *ApJ*, 738, 122
- Collier Cameron, A., Pollacco, D., Street, R. A., et al. 2006, *MNRAS*, 373, 799
- Cutri, R. M., Skrutskie, M. F., van Dyk, S., et al. 2003a, 2MASS Point Source Catalogue (available at <http://www.ipac.caltech.edu/2mass/>)
- Cutri, R. M., Skrutskie, M. F., van Dyk, S., et al. 2003b, *yCat*, 2246, 0
- David, M., Hensberge, H., & Nitschelm, C. 2014, *JAD*, 20, 1
- Dawson, P., Scholz, A., & Ray, T. P. 2011, *MNRAS*, 418, 1231
- de Geus, E. J., de Zeeuw, P. T., & Lub, J. 1989, *A&A*, 216, 44
- de Zeeuw, P. T., Hoogerwerf, R., de Bruijne, J. H. J., Brown, A. G. A., & Blaauw, A. 1999, *AJ*, 117, 354
- Douglas, S. T., Agüeros, M. A., Covey, K. R., et al. 2016, *ApJ*, 822, 47
- Erickson, K. L., Wilking, B. A., Meyer, M. R., Robinson, J. G., & Stephenson, L. N. 2011, *AJ*, 142, 140
- Gaia* Collaboration, Prusti, T., de Bruijne, J. H. J., et al. 2016, *A&A*, 595, A1
- Gallet, F., & Bouvier, J. 2013, *A&A*, 556, A36
- Gallet, F., & Bouvier, J. 2015, *A&A*, 577, A98
- Girard, T. M., van Alstena, W. F., Zacharias, N., et al. 2011, *AJ*, 142, 15
- Gontcharov, G. A. 2008, *AstL*, 34, 785
- Grankin, K. N., Zakirov, M. M., Arzumanyants, G. C., & Melnikov, S. Y. 1996, *IBVS*, 4405
- Guinan, E. F., & Dewarf, L. E. 2002, in ASP Conf. Ser. 279, Exotic Stars as Challenges to Evolution, ed. C. A. Tout & W. van Hamme (San Francisco, CA: ASP), 121
- Hartman, J. D., Gaudi, B. S., Holman, M. J., et al. 2008, *ApJ*, 675, 1254
- Hartman, J. D., Bakos, G. Á, Kovács, G., & Noyes, R. W. 2010, *MNRAS*, 408, 475
- Henden, A. A., Levine, S. E., Terrell, D., Smith, T. C., & Welch, D. 2012, *JAVSO*, 40, 430
- Henden, A. A., Templeton, M., Terrell, D., et al. 2016, *yCat*, 2336, 0
- Høg, E., Fabricius, C., Makarov, V. V., et al. 2000, *A&A*, 355, L27
- Hoogerwerf, R., de Bruijne, J. H. J., & de Zeeuw, P. T. 2000, *ApJL*, 544, L133
- Houk, N. 1978, Michigan Catalogue of Two-dimensional Spectral Types for the HD Stars, Vol. 2, Declinations $-53^\circ 0'$ to $-40^\circ 0'$ (Ann Arbor, MI: Univ. of Michigan)
- Houk, N. 1982, Michigan Catalogue of Two-dimensional Spectral Types for the HD Stars, Vol. 3, Declinations $-40^\circ 0'$ to $-26^\circ 0'$ (Ann Arbor, MI: Univ. of Michigan)
- Houk, N., & Smith-Moore, M. 1988, Michigan Catalogue of Two-dimensional Spectral Types for the HD Stars, Vol. 4, Declinations $-26^\circ 0'$ to $-12^\circ 0'$ (Ann Arbor, MI: Univ. of Michigan)
- Hughes, J., Hartigan, P., Krautter, J., & Kelemen, J. 1994, *AJ*, 108, 1071
- Hunter, J. D. 2007, *CSE*, 9, 3
- Irwin, J., Berta, Z. K., Burke, C. J., et al. 2011, *ApJ*, 727, 56
- Jones, E., Oliphant, T., Peterson, P., et al. 2001, SciPy: Open source scientific tools for Python
- Kenworthy, M. A., & Mamajek, E. E. 2015, *ApJ*, 800, 126
- Köhler, R., Kunkel, M., Leinert, C., & Zinnecker, H. 2000, *A&A*, 356, 541
- Kraft, R. P. 1967, *ApJ*, 150, 551
- Kraus, A. L., Cody, A. M., Covey, K. R., et al. 2015, *ApJ*, 807, 3
- Krautter, J., Wichmann, R., Schmitt, J. H. M. M., et al. 1997, *A&AS*, 123, 329
- Lodieu, N., Dobbie, P. D., Cross, N. J. G., et al. 2013, *MNRAS*, 435, 2474
- Lodieu, N., Hambly, N. C., & Jameson, R. F. 2006, *MNRAS*, 373, 95

- Lodieu, N., Hambly, N. C., Jameson, R. F., et al. 2007, *MNRAS*, **374**, 372
- Loinard, L., Torres, R. M., Mioduszewski, A. J., & Rodríguez, L. F. 2008, *ApJL*, **675**, L29
- Lombardi, M., Lada, C. J., & Alves, J. 2008, *A&A*, **480**, 785
- Luhman, K. L., & Mamajek, E. E. 2012, *ApJ*, **758**, 31
- Makarov, V. V. 2007, *ApJS*, **169**, 105
- Mamajek, E. E. 2008, *AN*, **329**, 10
- Mamajek, E. E., & Hillenbrand, L. A. 2008, *ApJ*, **687**, 1264
- Mamajek, E. E., Meyer, M. R., & Liebert, J. 2002, *AJ*, **124**, 1670
- Mamajek, E. E., Quillen, A. C., Pecaut, M. J., et al. 2012, *AJ*, **143**, 72
- Martín, E. L., Delfosse, X., & Guieu, S. 2004, *AJ*, **127**, 449
- McKinney, W. 2010, in Proc. of the 9th Python in Science Conference (SciPy 2010), Data Structures for Statistical Computing in Python, ed. S. van der Walt & J. Millman, 51, <http://conference.scipy.org/proceedings/scipy2010/mckinney.html>
- Meibom, S., Barnes, S. A., Platais, I., et al. 2015, *Natur*, **517**, 589
- Meibom, S., Mathieu, R. D., Stassun, K. G., Liebesny, P., & Saar, S. H. 2011a, *ApJ*, **733**, 115
- Meibom, S., Barnes, S. A., Latham, D. W., et al. 2011b, *ApJL*, **733**, L9
- Messina, S., Desidera, S., Turatto, M., Lanzafame, A. C., & Guinan, E. F. 2010, *A&A*, **520**, A15
- Meyer, M. R., & Wilking, B. A. 2009, *PASP*, **121**, 350
- Mikolajewski, M., & Graczyk, D. 1999, *MNRAS*, **303**, 521
- Morales-Calderón, M., Stauffer, J. R., Stassun, K. G., et al. 2012, *ApJ*, **753**, 149
- Morau, E., Artemenko, S., Bouvier, J., et al. 2013, *A&A*, **560**, A13
- Nutter, D., Ward-Thompson, D., & André, P. 2006, *MNRAS*, **368**, 1833
- Ortiz-León, G. N., Loinard, L., Kounkel, M. A., et al. 2017, *ApJ*, **834**, 141
- Pecaut, M. J., & Mamajek, E. E. 2013, *ApJS*, **208**, 9
- Pecaut, M. J., & Mamajek, E. E. 2016, *MNRAS*, **461**, 794
- Pecaut, M. J., Mamajek, E. E., & Bubar, E. J. 2012, *ApJ*, **746**, 154
- Perevozskina, E. L., & Svechnikov, M. A. 2004, *yCat*, **5118**, 0
- Perryman, M. A. C., Lindegren, L., Kovalevsky, J., et al. 1997, *A&A*, **323**, L49
- Pollacco, D. L. 2006, *PASP*, **118**, 1407
- Preibisch, T., Guenther, E., Zinnecker, H., et al. 1998, *A&A*, **333**, 619
- Preibisch, T., & Mamajek, E. 2008, in Handbook of Star Forming Regions, Volume II: The Southern Sky ASP Monograph Publications, ed. B. Reipurth (Vol. 5; San Francisco, CA: ASP), 235
- Press, W. H., Teukolsky, S. A., Vetterling, W. T., & Flannery, B. P. 1992, Numerical Recipes in FORTRAN. The Art of Scientific Computing (2nd ed.; Cambridge: Cambridge Univ. Press)
- Prša, A., Harmanec, P., Torres, G., et al. 2016, *AJ*, **152**, 41
- Reiners, A., & Mohanty, S. 2012, *ApJ*, **746**, 43
- Riaz, B., Gizis, J. E., & Harvin, J. 2006, *AJ*, **132**, 866
- Richards, J. W., Starr, D. L., Miller, A. A., et al. 2012, *ApJS*, **203**, 32
- Rizzuto, A. C., Ireland, M. J., & Kraus, A. L. 2015, *MNRAS*, **448**, 2737
- Rizzuto, A. C., Ireland, M. J., & Zucker, D. B. 2012, *MNRAS*, **421**, L97
- Rybka, S. P. 2007, *KFNT*, **23**, 102
- Sartori, M. J., Lépine, J. R. D., & Dias, W. S. 2003, *A&A*, **404**, 913
- Scargle, J. D. 1982, *ApJ*, **263**, 835
- Scott, E. L., Mamajek, E. E., Pecaut, M. J., et al. 2014, *ApJ*, **797**, 6
- Siess, L., Dufour, E., & Forestini, M. 2000, *A&A*, **358**, 593
- Skrutskie, M. F., Cutri, R. M., Stiening, R., et al. 2006, *AJ*, **131**, 1163
- Slesnick, C. L., Carpenter, J. M., Hillenbrand, L. A., & Mamajek, E. E. 2006, *AJ*, **132**, 2665
- Slettebak, A. 1955, *ApJ*, **121**, 653
- Smith, A. M. S. & WASP Consortium 2014, *CoSka*, **43**, 500
- Song, I., Zuckerman, B., & Bessell, M. S. 2012, *AJ*, **144**, 8
- Spencer Jones, H., & Jackson, J. 1936, Proper Motions of Stars in the Zone Catalogue -40 to -52 degrees of 20843 Stars for 1900 (London: HMSO)
- Struve, O., & Straka, W. C. 1962, *PASP*, **74**, 474
- Torres, C. A. O., Quast, G. R., da Silva, L., et al. 2006, *A&A*, **460**, 695
- Van Der Walt, S., Colbert, S.C., & Varoquaux, G. 2011, *CSE*, **13**, 22
- van Leeuwen, F. 2007, Hipparcos, the New Reduction of the Raw Data: Astrophysics and Space Science Library (Vol. 350; Dordrecht: Springer)
- Vrba, F. J., Strom, S. E., & Strom, K. M. 1976, *AJ*, **81**, 958
- Watson, C. L. 2006, *SASS*, **25**, 47
- Wichmann, R., Sterzik, M., Krautter, J., Metanomski, A., & Voges, W. 1997, *A&A*, **326**, 211